

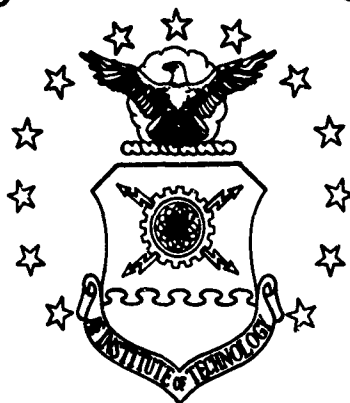
# UNCLASSIFIED

AD NUMBER
AD857523
NEW LIMITATION CHANGE
TO Approved for public release, distribution unlimited
FROM Distribution authorized to U.S. Gov't. agencies and their contractors; Critical Technology; JUN 1969. Other requests shall be referred to Air Force Inst. of Technology, Wright-Patterson AFB, OH 45433.
AUTHORITY
AFIT ltr, 22 Jul 1971

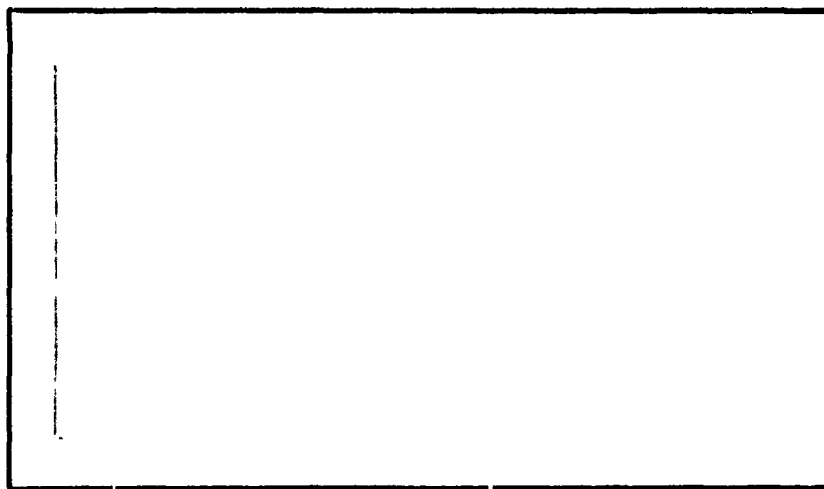
THIS PAGE IS UNCLASSIFIED

AD857523

# AIR FORCE INSTITUTE OF TECHNOLOGY

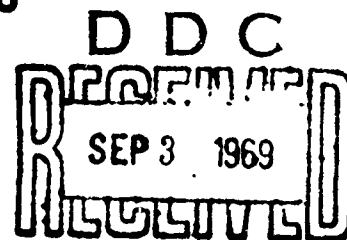


AIR UNIVERSITY  
UNITED STATES AIR FORCE



## SCHOOL OF ENGINEERING

WRIGHT-PATTERSON AIR FORCE BASE, OHIO



GNE/PH/69-4

ENERGY DEPENDENCE OF  
HIGH LATITUDE ELECTRON CUTOFFS  
THESIS

GNE/PH/69-4      Robert N. Davie, Jr.  
Lieutenant    USAF

This document is subject to special export controls and each transmittal to foreign governments or foreign nationals may be made only with prior approval of the Dean of Engineering, Air Force Institute of Technology (AFIT-SE), Wright-Patterson Air Force Base, Ohio, 45433

**GNE/PH/69-4**

**ENERGY DEPENDENCE OF  
HIGH LATITUDE ELECTRON CUTOFFS**

**THESIS**

**Presented to the Faculty of the School of Engineering of  
the Air Force Institute of Technology  
Air University  
in Partial Fulfillment of the  
Requirements for the Degree of  
Master of Science**

**by**

**Robert Nelson Davie, Jr., B.S.  
Lieutenant                      USAF**

**Graduate Nuclear Engineering**

**June 1969**

**This document is subject to special export controls and  
each transmittal to foreign governments or foreign na-  
tionals may be made only with prior approval of the Dean  
of Engineering, Air Force Institute of Technology (AFIT-  
SE), Wright-Patterson Air Force Base, Ohio, 45433**

### Preface

This thesis represents six months of research in the Particles and Fields Division of the Space Physics Laboratory at Aerospace Corporation as a part of the AFIT masters degree program. During this time I analyzed satellite data to gain information about outer belt electron behavior and the magnetosphere.

Knowledge of the radiation belt is important both to science and the Air Force. To science it represents a better understanding of our environment. To the Air Force, which is presently concerned with manned orbital flight it represents knowledge about one of the hazards encountered in space. It is important to precisely know the radiation hazards in order to protect both men and equipment from damage.

The personnel of the Space Physics Lab provided me with immense support and for this I am deeply indebted. Virtually every individual played some part in making this thesis possible and I wish to thank them all. I would specifically like to recognize Dr. Albert Vampola and Dr. George Paulikas. They not only gave me key advice and guidance throughout my research but made my stay a learning experience extending well beyond the area of my specific topic. I thank them both for their valuable time and effort.

I would like to specially thank Lt. Col. Donald L. Evans both for his valuable assistance as my AFIT thesis advisor and for making this valuable learning experience possible. I also acknowledge the as-

**GNE/PH/69-4**

**sistance extended me by Lt. David J. Evans of SAMSO.**

Contents

Preface . . . . .	ii
List of Figures . . . . .	v
List of Tables . . . . .	viii
Abstract . . . . .	ix
I. Introduction . . . . .	1
II. Background . . . . .	5
III. Data Analysis . . . . .	18
IV. Conclusions . . . . .	49
V. Suggestions for Future Investigation . . . . .	59
Bibliography . . . . .	61
Appendix A: The Instrument . . . . .	63
Appendix B: Error Propagation . . . . .	67
Vita . . . . .	69

## List of Figures

Figure		Page
1	Plot of Electron Flux Versus L for Rev 206, August 24, 1966 . . . . .	2
2	Model of the Magnetosphere Showing the Areas Being Examined in this Study . . . . .	3
3	Perfect Dipole Representation of the Earth's Magnetic Field . . . . .	6
4	Charged Particle Motion in the Earth's Magnetosphere . . . . .	7
5	B and L Mapping of the Earth's Magnetic Field . . . . .	9
6	The Williams and Mead Model of the Magnetosphere . . . . .	11
7	High Latitude Cutoffs as a Function of Magnetic Local Time found by McDiarmid and Burrows from Alouette 2 Data . . . . .	14
8	The Instrument . . . . .	15
9	Flight Characteristics of the OV3-3 Satellite . . . . .	17
10	Plot of $J_1$ Versus Universal Time for Rev 1991 February 9, 1967 . . . . .	19
11	Plot of $J_1$ Versus Universal Time for Rev 1926, February 3, 1967 which Shows Solar Flare Electrons . . . . .	23
12	Types of Spike Phenomenon Observed During Magnetically Disturbed Periods . . . . .	25
13	Plot of Cutoff Versus Altitude for Channel 7 . . . . .	28
14	Plot of Cutoff Versus Local Time for Channel 7 . . . . .	29
15	Plot of Cutoff Versus the 3 hr Average $K_p$ Index for Channel 8 . . . . .	30



16	Plot of Cutoffs Averaged Over Half Hour Intervals and Associated Standard Deviations as a Function of Local Time for Channel 8 . . . . .	32
17	Ninth Order Fit to the Average Cutoff Versus Local Time Plot Redundantly Extended Over 48 Hours . . . .	33
18	Fourth Order Fit to Ninth Order Curve Over the Interval 12 to 36 Hours Corrected Back to 0 to 24 Hours and Compared with Data . . . . .	36
19	Plot of Empirical Fits to the Cutoff Versus Local Time Plots for Channels 2 through 9 . . . . .	37
20	Plot of Diurnal Variation of Cutoff as a Function of the Higher Cutoff for Matched Pass Data from all Channels with One Data Point Falling in the Local Time Interval of 0000-0200 Hours . . . . .	39
21	Plot of Diurnal Variation of Cutoff as a Function of the Lower Cutoff for Matched Pass Data from all Channels with One Data Point Falling in the Local Time Interval of 0000-0200 Hours . . . . .	40
22	Plot of Diurnal Variation of Cutoff as a Function of the Average Cutoff for Matched Pass Data from all Channels with One Data Point Falling in the Local Time interval of 0000-0200 Hours . . . . .	41
23	Plot of Local Time Corrected Cutoff Versus the 3 Hour Average $K_p$ Index for Channel 7 with No Time Lag . . . . .	43
24	Plot of Local Time Corrected Cutoffs Averaged Over $K_p$ Index for Channel 7 with No Time Lag . . . .	44
25	Plot of Local Time Corrected Cutoff Versus Dst for Channel 9 with No Time Lag . . . . .	46
26	Plot of Local Time Corrected Cutoffs Averaged Over 5 Gamma Intervals Versus Dst for Channel 9 with No Time Lag . . . . .	47

27	Plot of Local Time Corrected Cutoffs Averaged Over 5 Gamma Intervals Versus Dst for Channel 9 for All 10 Time Lags from 5 Hours Before to 5 Hours After the Observation . . . . .	48
28	Angle of Solar Wind Interaction with the Magnetosphere .	50
29	The Magnetosphere Showing Kinks in the Closed Field Lines of the Tail . . . . .	54
30	Predicted and Observed High Latitude Electron Cutoffs as a Function of Energy . . . . .	51
31	Predicted and Observed Diurnal Variations of Cutoffs as a Function of the Day or Night Cutoff . . . . .	58

List of Tables

Table	Page
I    Data on High Latitude Spikes . . . . .	26
II   Coefficients for the Expression of the Cutoff as a Function of Local Time . . . . .	35
III   Characteristics of Detectors . . . . .	65

Abstract

The high latitude electron cutoffs are determined from electron flux data collected by the magnetic spectrometer aboard the polar orbiting OV3-3 satellite (1966-70A). The cutoffs are examined as a function of nine energies from 300 keV to 2.3 MeV and are found to be a function of energy for all local times and to exhibit an energy dependent diurnal variation. This phenomenon is explained with the use of the models of Taylor and Hones and of Williams and Mead. The lower energy cutoffs occurring at higher latitudes is purported to result from kinks in the nightside magnetic field lines and the limiting effect of rigidity. The greater diurnal variation for the lower energy cutoffs is thought to be the result of field distortion with the different energies labeling different L shells. The cutoffs show no altitude dependence and no well defined relationship with magnetic activity as represented by either Dst or Kp.

## ENERGY DEPENDENCE OF HIGH LATITUDE ELECTRON CUTOFFS

### I. Introduction

The radiation belt surrounding the earth was first discovered by Van Allen, Ludwig, Ray and McIlwain in 1958 (Ref. 3:220). The belt was shown to contain both electrons and protons (Ref. 4:16). A mapping of the electrons in the radiation belt show that for high energy electrons the belt consists of two zones, while for lower energies the distribution is almost continuous to about 10 earth radii at the equator. For energetic electrons the inner zone extends to around 2 earth radii and the outer zone from about 3 to 10 earth radii. This is shown in Figure 1. In the inner and outer zones, source, loss, acceleration and diffusion mechanisms still remain quantitatively uncertain.

The present study is an investigation of trapped electron behavior in the outer fringes of the outer zone at low altitudes. The high latitude cutoff of trapped electrons is examined to gain information about outer zone electron behavior and the magnetosphere. Observing the outer zone electrons yields clues as to what is going on in the outer portions of the magnetosphere. The high latitude cutoffs are important in examining the trapping boundary or the limit of closed field lines in the magnetosphere. Figure 2 shows the relationship between

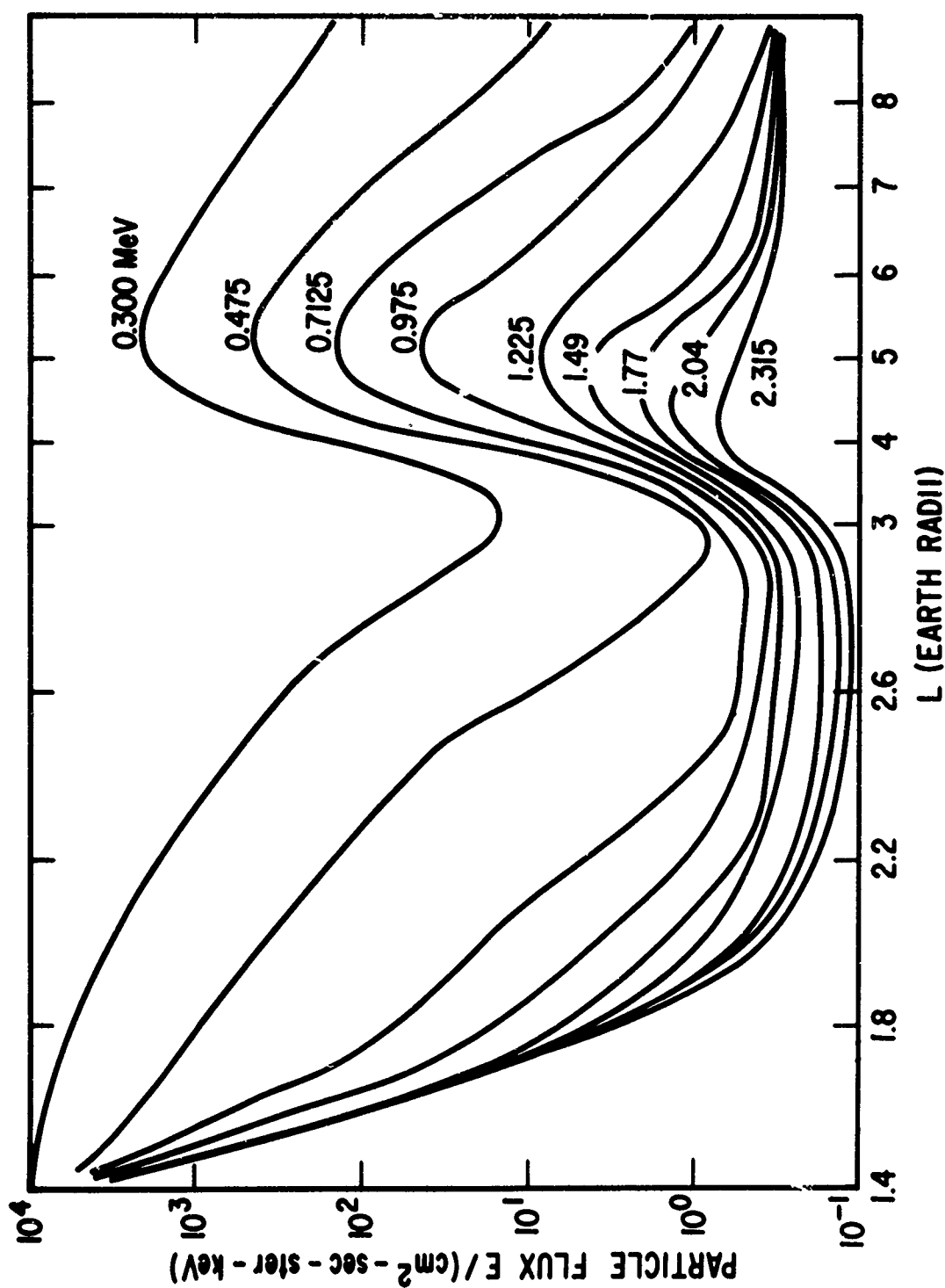


FIG. 1. PLOT OF ELECTRON FLUX versus L FOR REV 206, AUGUST 24, 1966

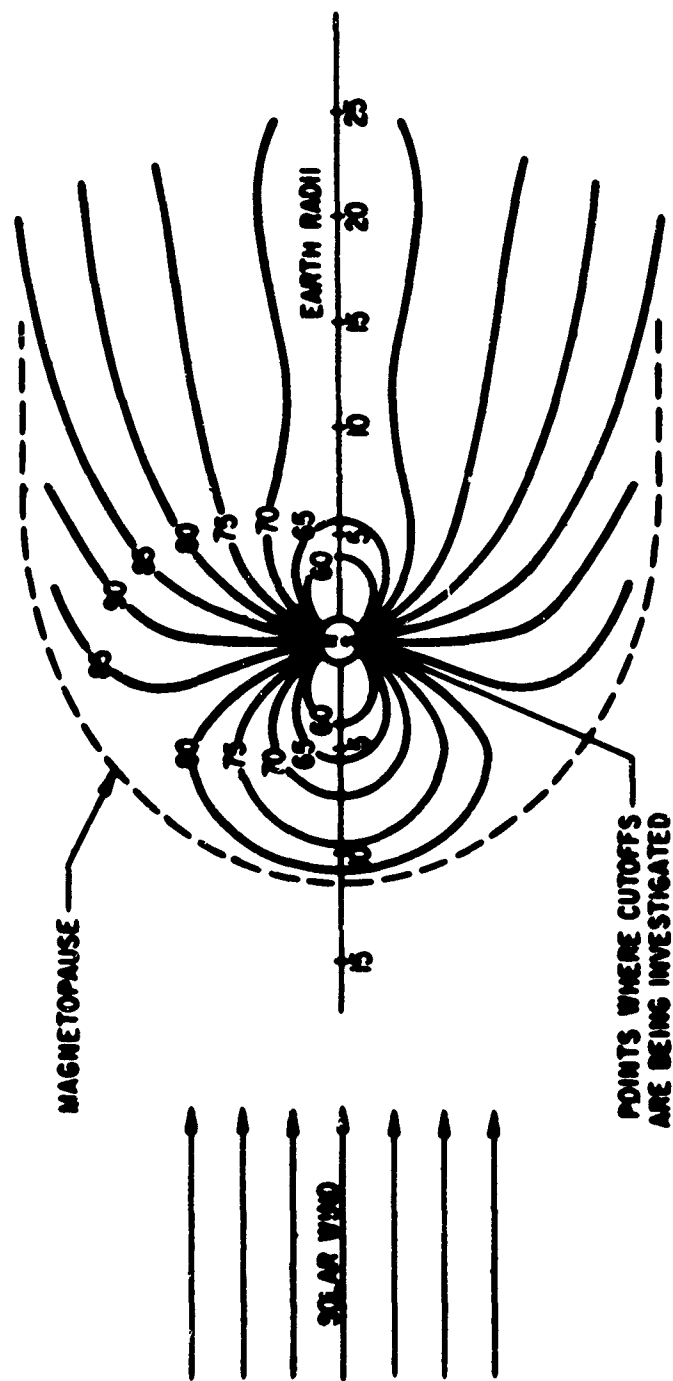


FIG. 2. MODEL OF THE MAGNETOSPHERE SHOWING THE AREAS BEING EXAMINED IN THIS STUDY

(FROM REF 16:3025)

the high latitude cutoff and the field lines of the magnetosphere. At present, the outer part of the magnetosphere is the least understood. Most magnetospheric models are valid close in to the earth, but this validity decreases rapidly beyond several earth radii. Information about the limit of closed field lines can be used as a boundary condition to evaluate and improve magnetospheric models.

This investigation is a systematic examination of the high latitude cutoffs from approximately 150 orbits of the OV3-3 polar orbiting satellite (1966-70A). The cutoffs are analyzed as a function of nine energies from 300 keV to 2.3 MeV and relationships with magnetic activity are examined. The computer is used extensively to facilitate examination of the available data.



## II. Background

Particle motion in the magnetosphere is briefly reviewed as a means of clarifying the significance of the high latitude cutoff of electrons. The magnetic field of the earth can be approximately represented as a dipole, as shown in Figure 3. A charged particle moving in such a field will have three distinct motions; the particle will spiral about a field line (cyclotron motion), bounce back and forth along the field line between two mirror points, and drift around the earth. (Ref. 4:23). These three motions are depicted in Figure 4. The approximate periods associated with these motions for a 1 MeV electron with a 2000 km altitude at the equator are  $10^{-6}$  sec for the cyclotron motion,  $10^{-1}$  sec for the bounce motion and 60 min for the drift motion (Ref. 4:34). This close association between these trapped particles and the magnetosphere make the behavior of the particles useful in investigating the magnetosphere.

The assumptions that the magnetic field is slowly varying with time and space yields three adiabatic invariants. The magnetic moment, the length of a particle's bounce path along a field line, and the magnetic flux enclosed by the drift path can be assumed constant if the time scale of any variation and spatial scale of any inhomogeneity in the magnetic field are large compared to those characteristic of the cyclotron, bounce, and drift motions, respectively. The result of the

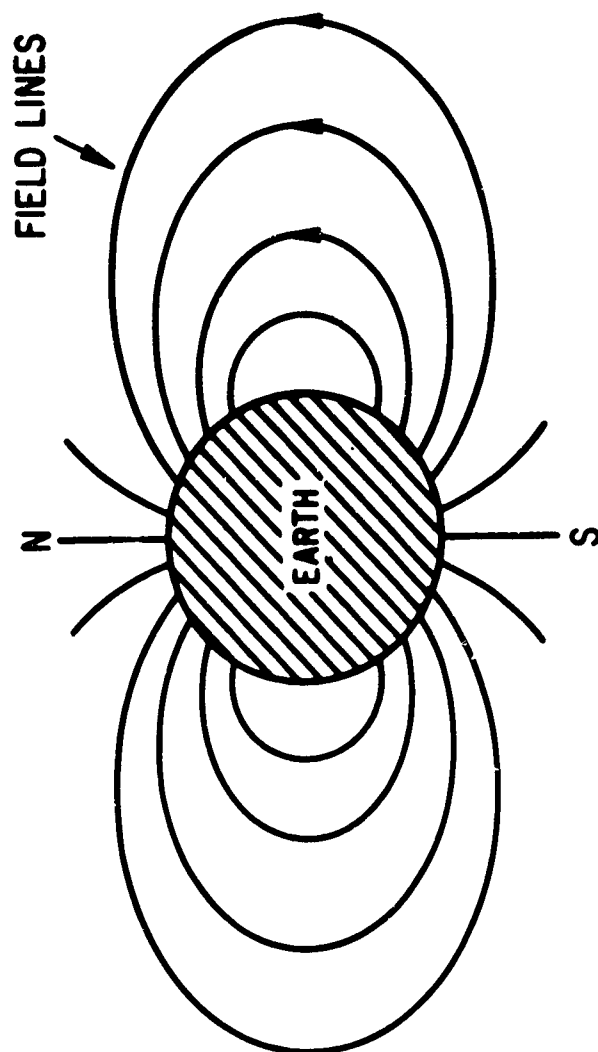


FIG. 3 . PERFECT DIPOLE REPRESENTATION OF THE EARTH'S MAGNETIC FIELD

(FROM REF 2:521)

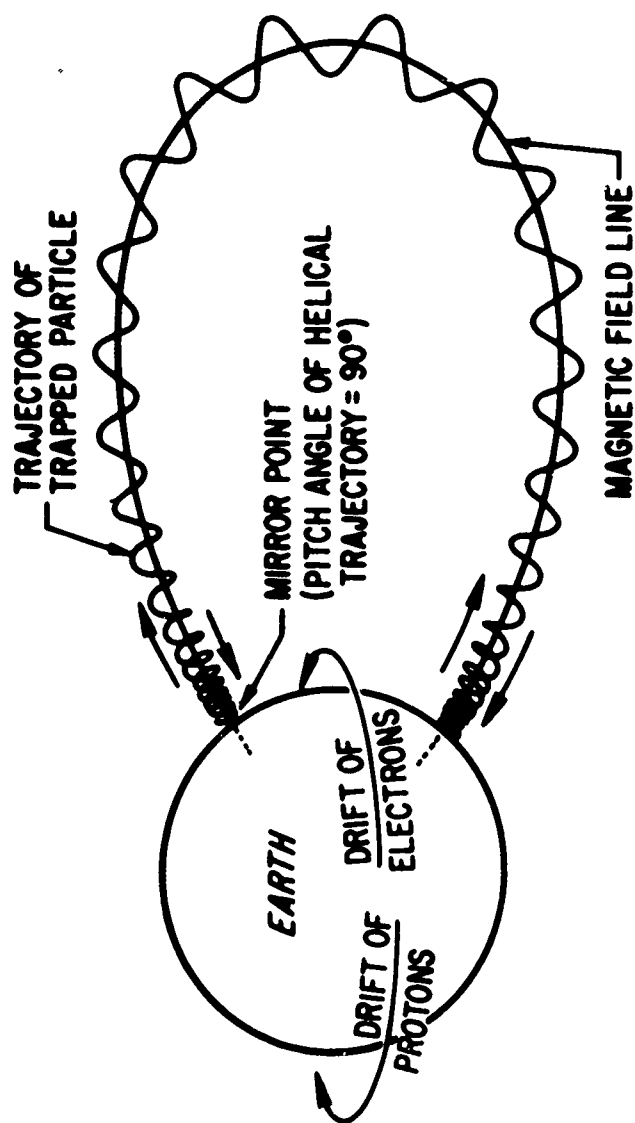


FIG. 4. CHARGED PARTICLE MOTION IN THE EARTH'S MAGNETOSPHERE

(FROM REF 4:28)

magnetic moment being constant is to require that the flux through a cyclotron orbit remain constant and that a specific particle will always mirror at the same value of the magnetic field.

These three adiabatic invariants are three constants of motion that one can use to describe a particle's motion in the actual dynamic field of the earth, assuming  $B$  changes little with time and space. However,  $B$  does change with time and space, and on occasion one or more of the invariants may be violated. The third is the most likely of the three to be violated since changes of the order of an hour are not unusual during magnetically active periods. There is evidence that the other invariants may also be violated.

To simplify the discussion and representation of trapped particles in the imperfect dipole field of the earth, McIlwain proposed using the value of the magnetic field,  $B$ , and the magnetic shell parameter,  $L$ , as coordinates. The advantage of this system is that a set of values of  $B$  and  $L$  correspond uniquely to one set of values of  $B$  and  $I$ , the integral invariant. A trapped particle ideally will always have the same  $L$  coordinate in this system as it drifts around the earth. For a dipole field,  $L$  is equal to the equatorial distance from the center of the earth to the field line, and for a nondipole field,  $L$  is the generalization of the equatorial distance, which turns out to be very nearly constant along a line of force.  $L$  varies by less than 1 percent along most field lines (Ref. 4:57-58). Figure 5 shows how the magnetosphere is described in the  $B$ - $L$  coordinate system.

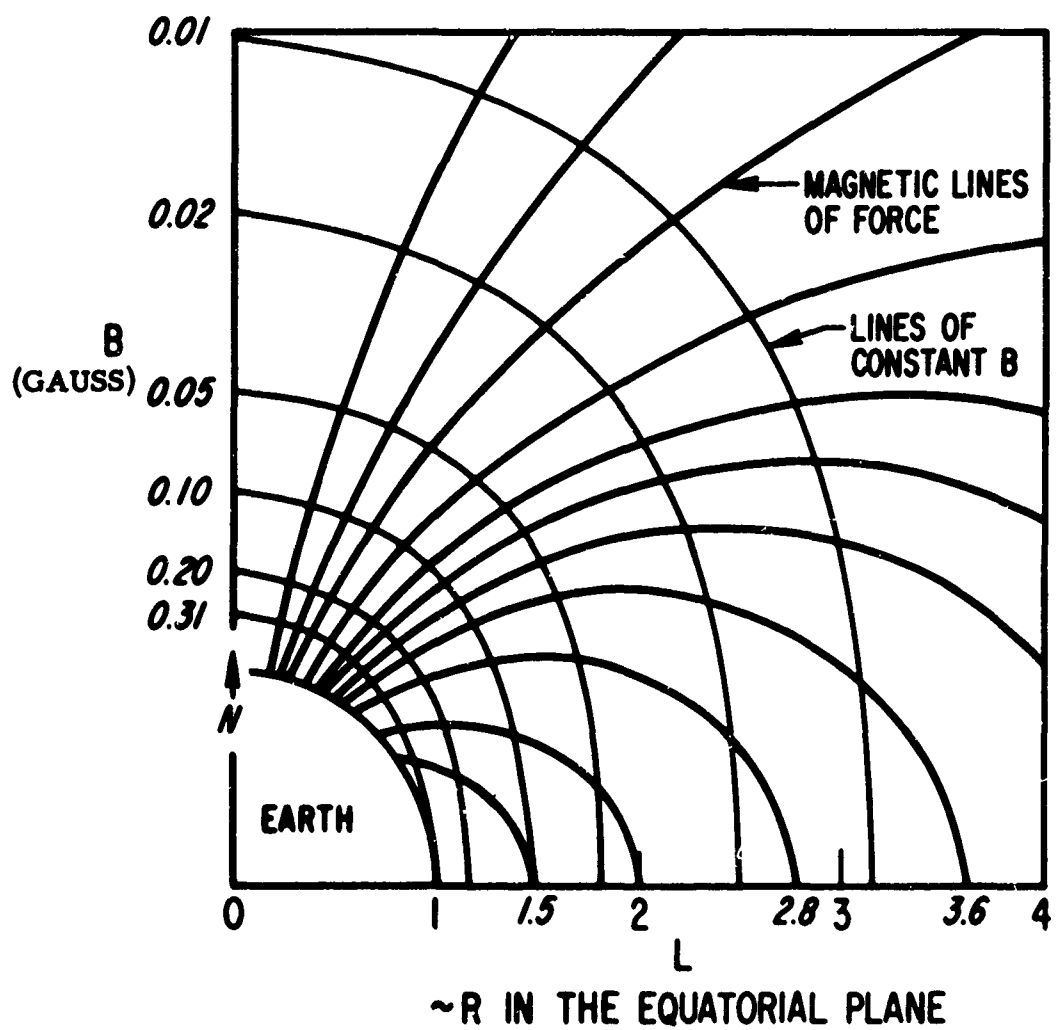


FIG. 5. B AND L MAPPING OF THE EARTH'S MAGNETIC FIELD

(FROM REF 3:193)

Associated with the B-L coordinate system is the invariant latitude,

$$\Lambda = \cos^{-1} \left( \frac{1}{L} \right)^{1/2} \quad (1)$$

This latitude can be considered very approximately as the latitude where the L shell intersects the earth. For an infinite L value,  $\Lambda = 90$  deg; for  $L = 1$ ,  $\Lambda = 0$  (Ref. 4:59).

The interaction of the solar wind and the geomagnetic field has been described by William and Mead. The solar wind compresses the field lines on the day side of the earth and extends those on the night side, as shown in Figure 6. The boundary between the solar wind and the magnetosphere on the day side is located at about  $10 R_e$  (Ref. 16:3024). On the night side, the effect of the solar wind is to cause field lines beyond about  $7 R_e$  to be open instead of closed. Also, for a given altitude above the earth, the value of B is greater on the day side than on the night side as a result of the solar wind compression of the field lines (Ref. 16:3025).

The high latitude cutoff of electrons is the invariant latitude above which trapped electrons are not observed. If closed field lines extend only to  $7 R_e$  on the night side of the earth and the boundary of the magnetosphere is at  $10 R_e$  on the day side, no particles should be trapped for  $L > 7$  on the night side or  $L > 10$  on the day side. From eq. (1) we can calculate the invariant latitudes corresponding to these two L values and the theoretical day side and night side high latitude

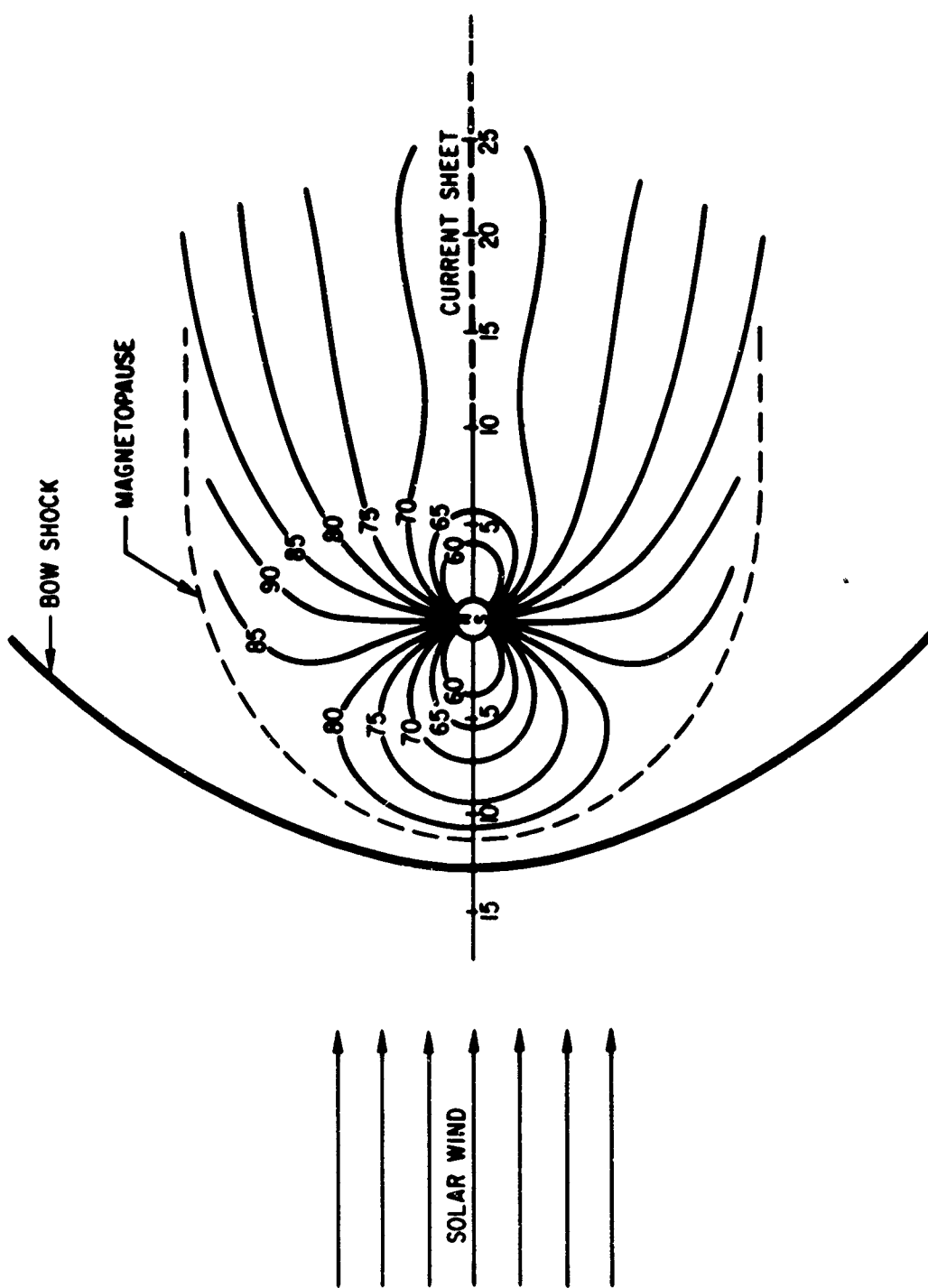


FIG. 6. THE WILLIAMS AND MEAD MODEL OF THE MAGNETOSPHERE

(FROM REF 16:3025)

cutoffs. They are approximately 71.5 deg invariant latitude on the day side and 68 deg on the night side. Actual measurements of the cutoffs, however, have shown that these calculations are not born out by experiment.

O'Brien discovered in 1963 that the high latitude cutoff for electrons with energy  $E > 40$  keV varied by several degrees according to the local time, with the highest values occurring in the local day. The cutoffs occurred at  $\approx 75$  deg around local noon and  $\approx 69$  deg around local midnight (Ref. 9:989).

In 1964, McDiarmid and Burrows, in examining Aloutte data for electron energy  $E > 40$  keV, found substantially the same diurnal variation in the cutoffs as O'Brien. They noted that the cutoffs were approximately symmetrical about the noon-midnight meridian (Ref. 6:616).

In 1965, Williams and Mead examined the high latitude boundaries for electrons of energies  $E > 280$  keV and  $E > 1.2$  MeV. They found a noon-midnight asymmetry of  $2 \frac{1}{2}$  deg which corresponds closely with the asymmetry predicted by invariant particle motion in a distorted magnetosphere. They concluded that the boundary was the same for electrons with energies  $E > 40$  keV,  $E > 280$  keV, and  $E > 1.2$  MeV at local midnight. However, the dayside cutoff for electrons  $E > 40$  keV consistently extended to higher latitudes than those for electrons with energies  $E > 280$  keV and  $E > 1.2$  MeV (Ref. 16:3028).

Also in 1965, Armstrong examined cutoffs from Injun 3 satel-



lite data and found the diurnal variation to be a function of energy. He investigated electrons with energies  $E > 40$  keV,  $E > 230$  keV, and  $E > 1.6$  MeV and noted that the diurnal variation decreased with increasing energy (Ref. 1:2101).

In 1968, McDiarmid and Burrows again examined the high latitude cutoffs as a function of energy and found that the  $E > 3.9$  MeV cutoffs were approximately symmetrical with respect to the 1100-2300 hr meridian and exhibited a diurnal variation of 3 deg. For  $E > 35$  keV electrons a diurnal variation of 6 deg was found, and the cutoffs were not symmetrical about any meridian. However, an appreciable dawn-dusk asymmetry was evident (Ref. 7:49). These trends can be seen in Figure 7.

The role of geomagnetic activity in influencing the high latitude cutoffs of electrons was examined by Maehlum and O'Brien in 1963. They found that during times of enhanced magnetic activity the boundary for electrons  $E > 40$  keV moved to lower latitudes for both night and day cutoffs. The cutoffs also became quite sharp during storms (Ref. 5:977-1000).

The present study is concerned with clarifying the above observations. The data used consist of magnetic spectrometer measurements of  $J_{\perp}$ , the electron flux perpendicular to the field line ( $\alpha = 90 \pm 8$  deg), for nine energies from 300 keV to 2.3 MeV. The instrument is shown in Figure 8. Its design, construction, and calibration were performed by A. L. Vampola at Aerospace Corporation and were not

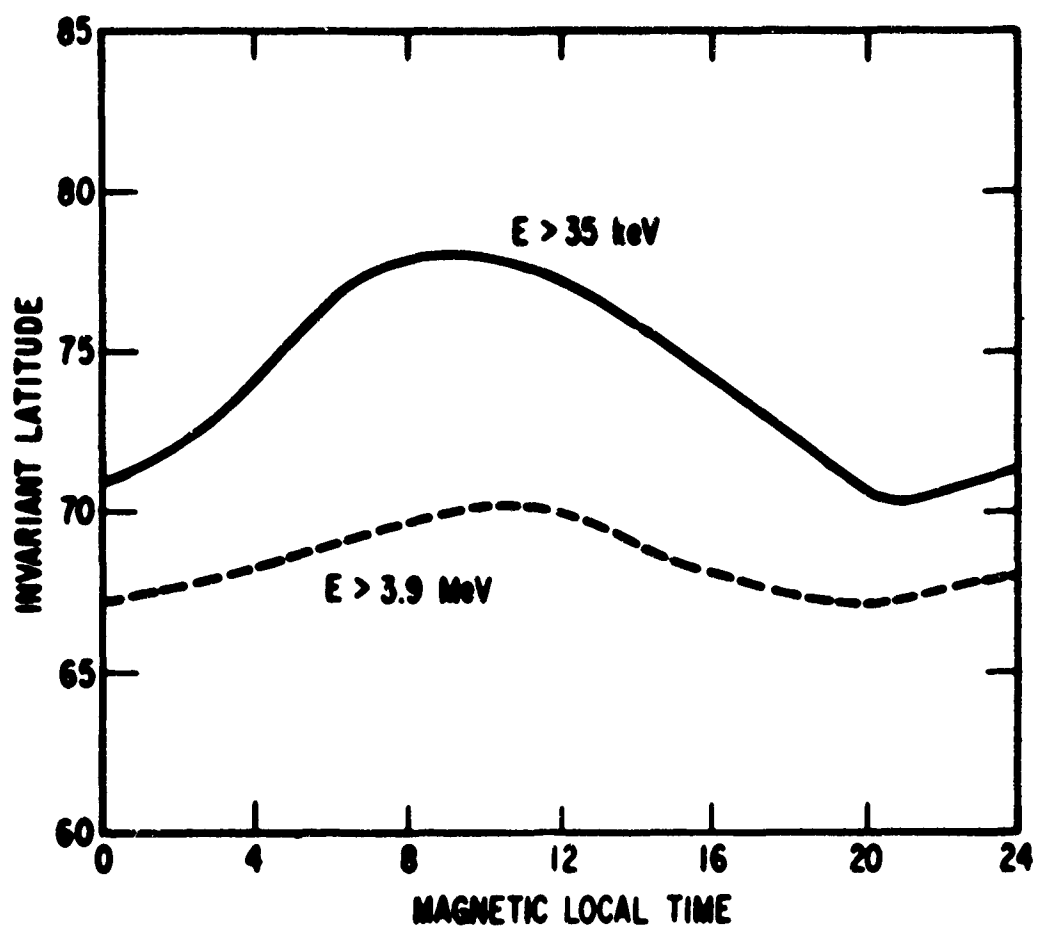


FIG. 7. HIGH LATITUDE CUTOFFS AS A FUNCTION OF MAGNETIC LOCAL TIME FOUND BY McDIARMID AND BURROWS FROM ALOUETTE 2 DATA

(FROM REF 7:53)

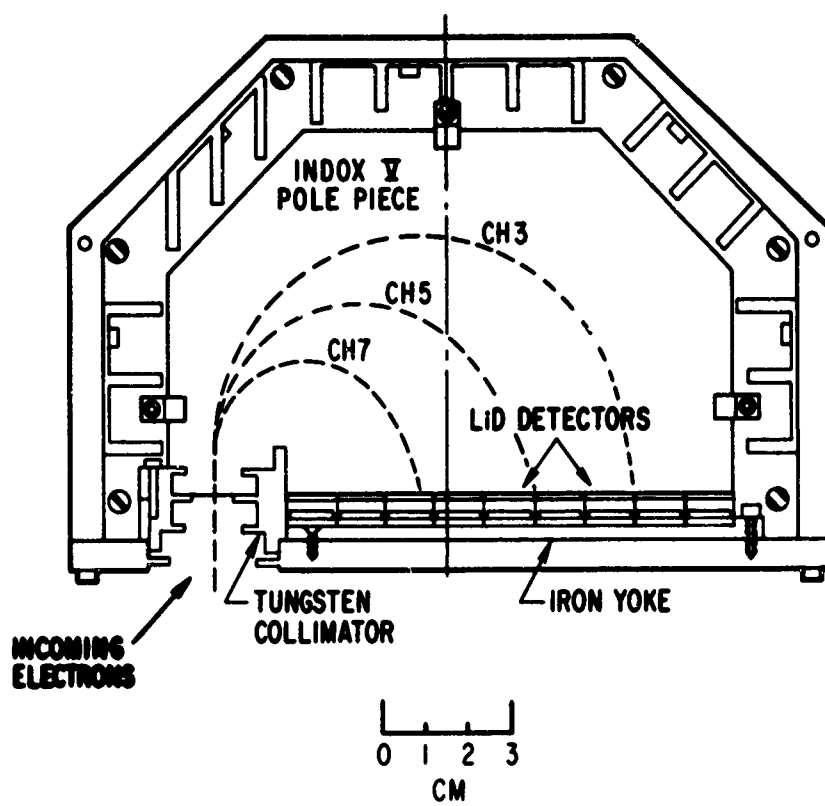


FIG. 8. THE INSTRUMENT  
(FROM REF: 14:37)

a part of this study. Details of the instrument's operation are discussed in Appendix A. The vehicle carrying the instrument was the OV3-3 polar satellite launched on 4 August 1966. The satellite had a period of 136.6 min, an inclination of 81.6 deg, a perigee of 200 nm, and an apogee of 2780 nm. A schematic of the satellite's trajectory is shown in Figure 9. The  $J_1$  data was merged with the ephemeris by computer, and plots of  $J_1$  versus universal time obtained for about 150 orbits. An example of these plots appears in Figure 10. The high latitude cutoffs used in this study were obtained from these plots.

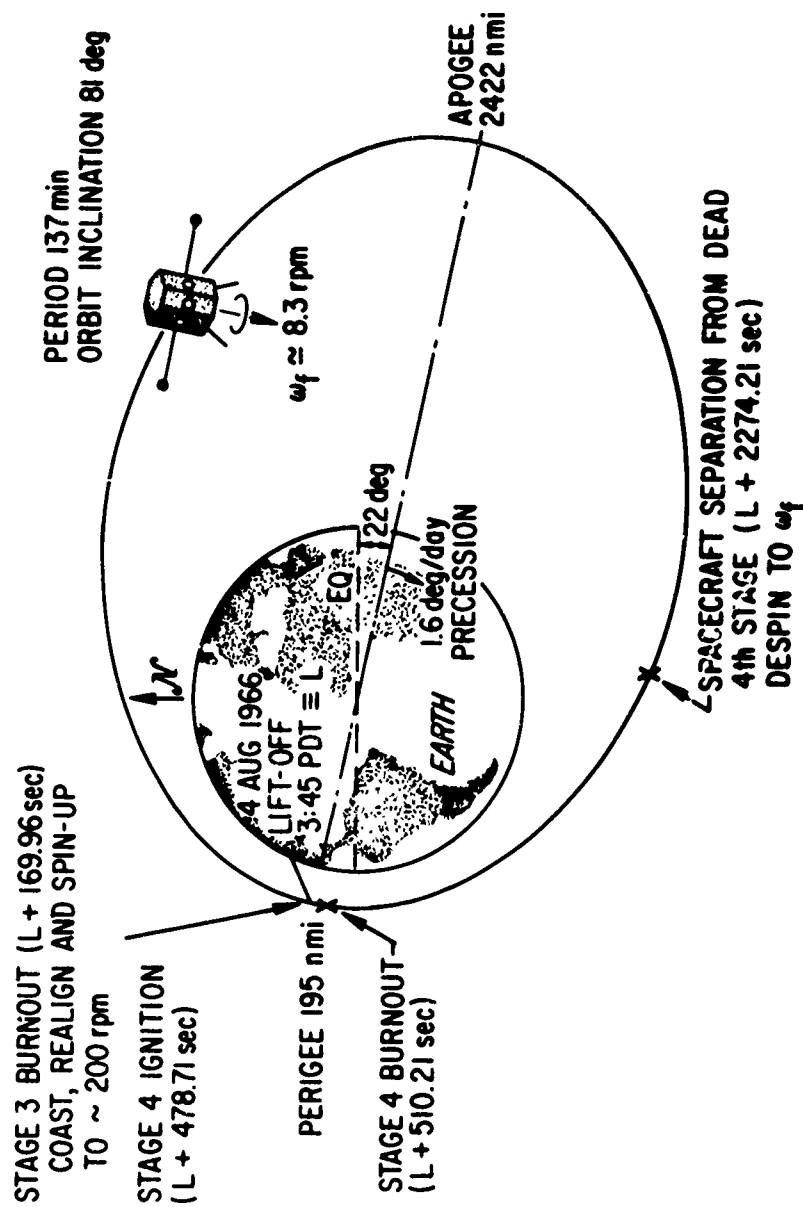


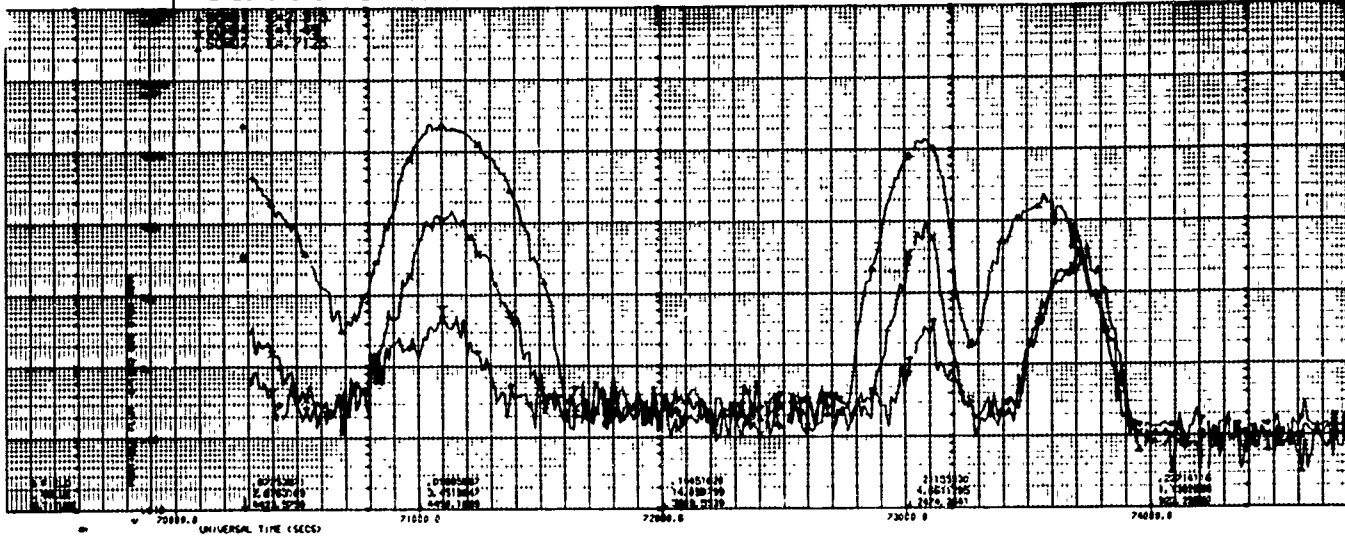
FIG. 9. FLIGHT CHARACTERISTICS OF THE OV3-3 SATELLITE

### III. Data Analysis

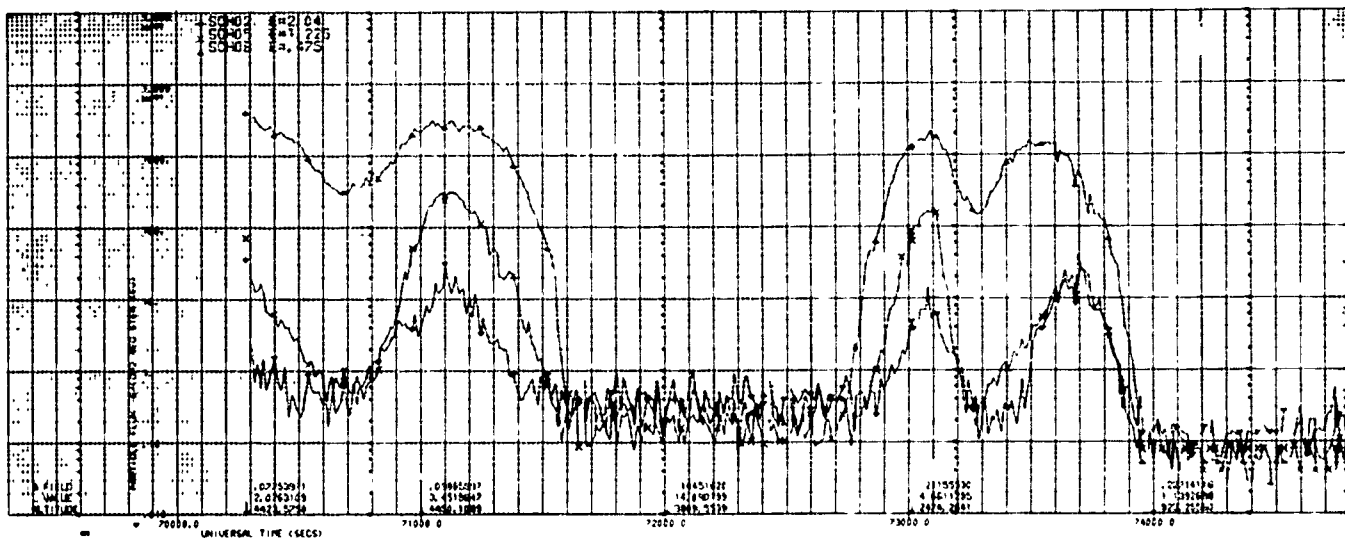
The problem of defining exactly where the high latitude cutoff occurs is not new. McDiarmid and Burrows dealt with this problem by defining and using several cutoffs. For example, they defined a background cutoff where the flux falls to the background level, a smooth cutoff where the flux profile shows a marked change in character, and a sharp cutoff where the flux decreases by a factor of ten or more in a latitude interval of less than half a degree (Ref. 7:50). Of the three, the only definition practical for this study was the first, or background, cutoff. Defining the cutoff at the point where the flux falls to a certain percentage of the maximum was considered, but any reasonable percentage eliminated too much data. The maximum flux values for the highest energy channels were often so low that taking five percent of these values yielded a flux value below background, making a cutoff point impossible to define. Taking ten or more percent of the maximum made the cutoff point too dependent upon the flux profile and therefore meaningless. Thus the cutoffs used in this study were defined as the invariant latitude at which  $J_{\perp}$ , the flux perpendicular to the local field line ( $\alpha = 90 \pm 8$  deg), assumed its background level.

Using a background cutoff was not without problems. The first was with cutoffs that were not extremely sharp. Where the flux curve

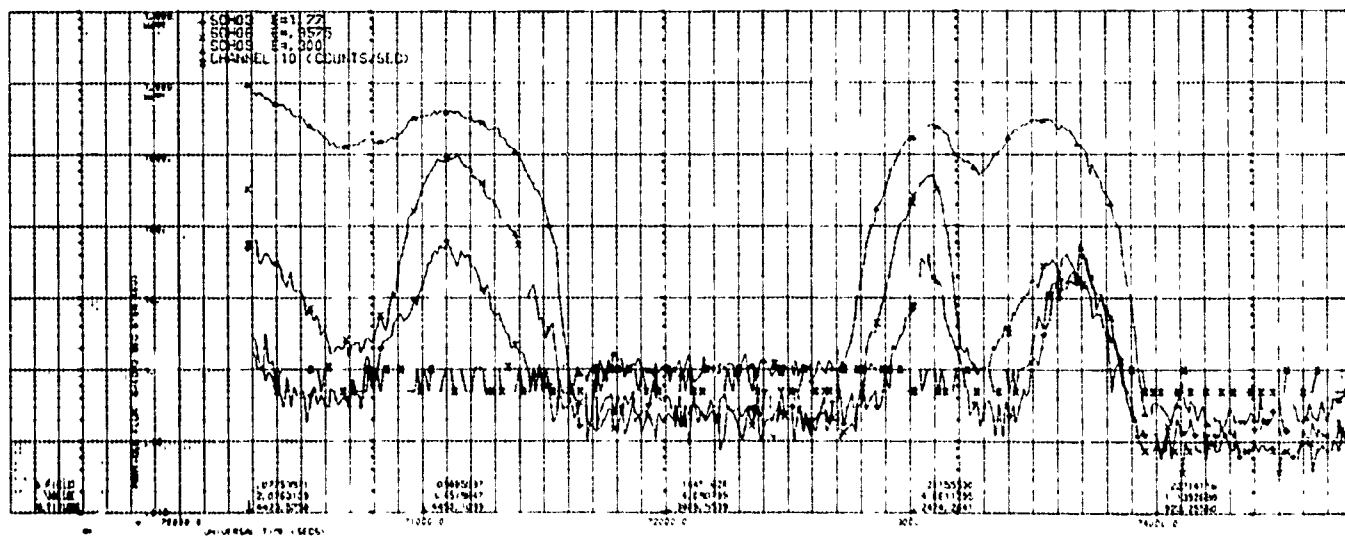
CHANNELS 1, 4, 7

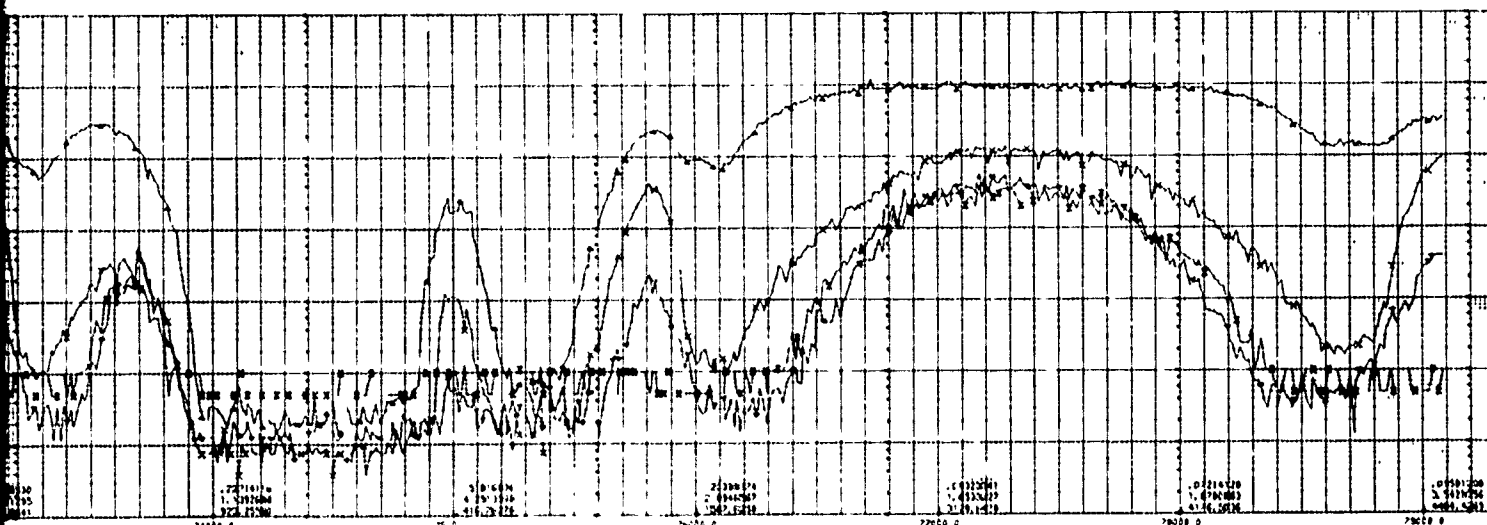
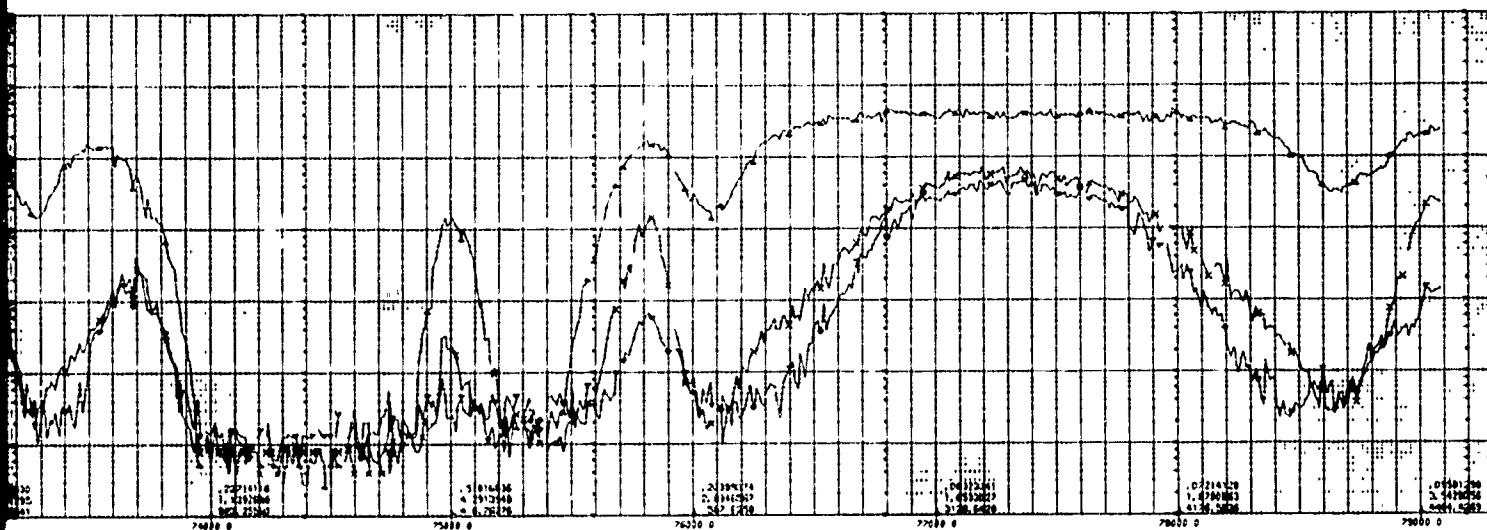
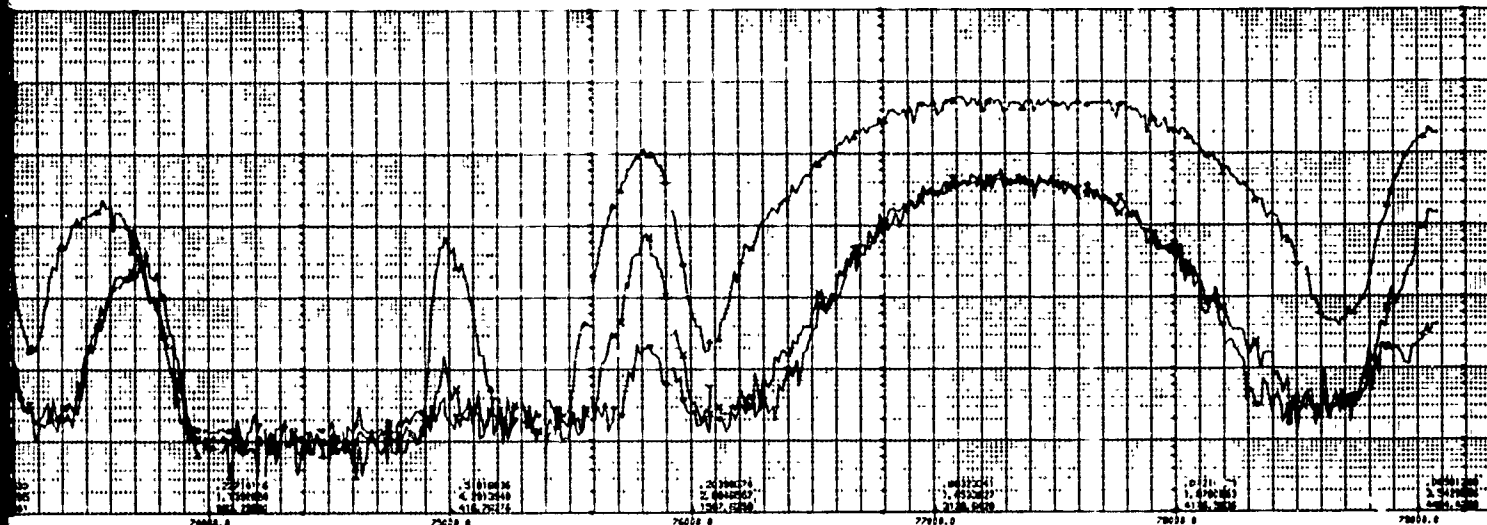


CHANNELS 2, 5, 8



CHANNELS 3, 6, 9

OUTER  
ZONENORTH  
POLEOUTER  
ZONEINNER  
ZONEPERIGEE  
(ATMOSPHERIC  
CUTOFF)FIG. 10. PLOT OF  $J_1$  versus UNIVERSAL TIME FO



▲  
INNER  
ZONE

▲  
PERIGEE  
(ATMOSPHERIC  
CUTOFF)

▲  
OUTER SOUTH  
POLE

▲  
OUTER  
ZONE

▲  
INNER  
ZONE

OF  $J_1$  versus UNIVERSAL TIME FOR REV 1991, FEBRUARY 9, 1967

B



slowly approached background, the statistical variation associated with the low background counting rates made determination of the exact cutoff point difficult. This problem was overcome by extrapolation of the flux curve down from an order of magnitude above the background level.

The second problem was the effect of solar flare electrons (Ref 14:1254) on the polar background levels. They increased the normal background levels by orders of magnitude for the lower energy channels, while the higher energies were relatively unaffected. This was overcome by simple extrapolation down to the observed background levels for each channel and accepting the decreased reliability of the data from the affected orbits. As shown in Figure 11, around a universal time of 56450 sec the shape of the flux curve has been altered, and it is difficult to say exactly where trapping stops.

Approximately 2800 cutoffs were defined. Each cutoff, along with the associated parameters of interest from the ephemeris, was put on cards to facilitate computer processing.

The cutoffs were usually sharper and better defined during local night than during local day. Also, in several instances low energy ( $\approx 300$  keV) spikes were seen above the cutoff latitude during magnetically disturbed periods. Even in some cases where no distinct spike was present, the cutoff shape was altered in such a way as to suggest a spike being barely enclosed by the cutoff. For example, the

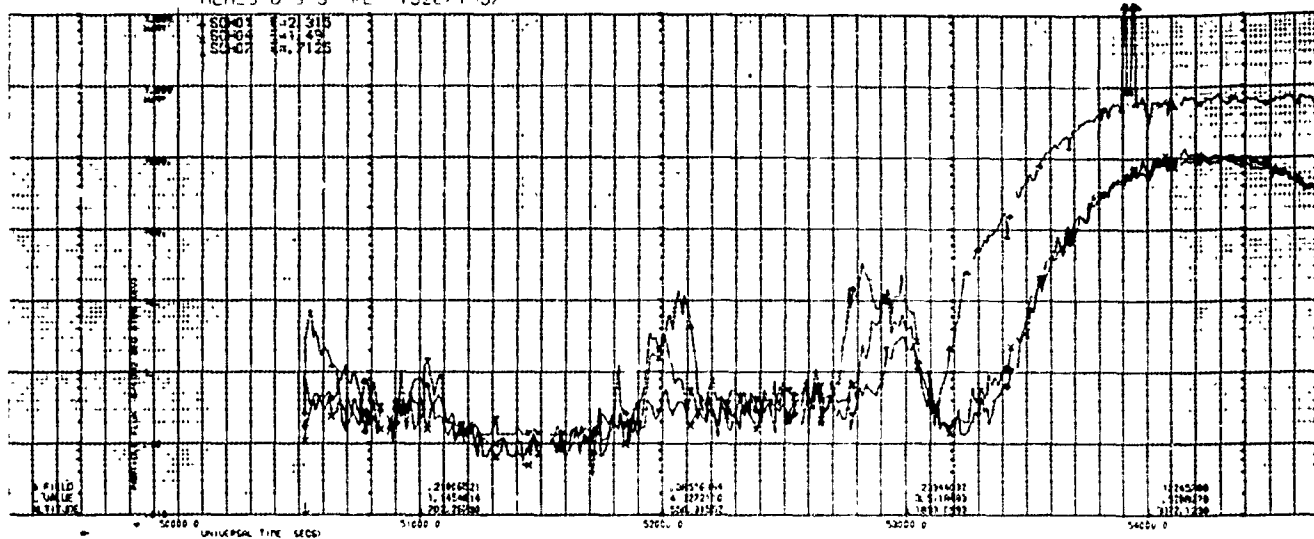
cutoff might appear pushed out and deformed just before the flux fell to background. Figure 12 shows these phenomena. The local times during which spikes were observed are listed in Table I. Most definite spikes occur around local midnight, while evidence of less definite spikes was observed mostly in the morning before noon. No conclusion with regard to the spikes was reached, and too few were observed to facilitate a detailed investigation.

There is one problem inherent in looking at cutoffs. When the cutoff is observed to be different for any two revolutions, the observer cannot say whether particles moved to different L shells or the L shells moved to different locations, because to get values for L and  $\Lambda$  we use a computerized magnetospheric model, which does not take into account all such variations in the magnetosphere.

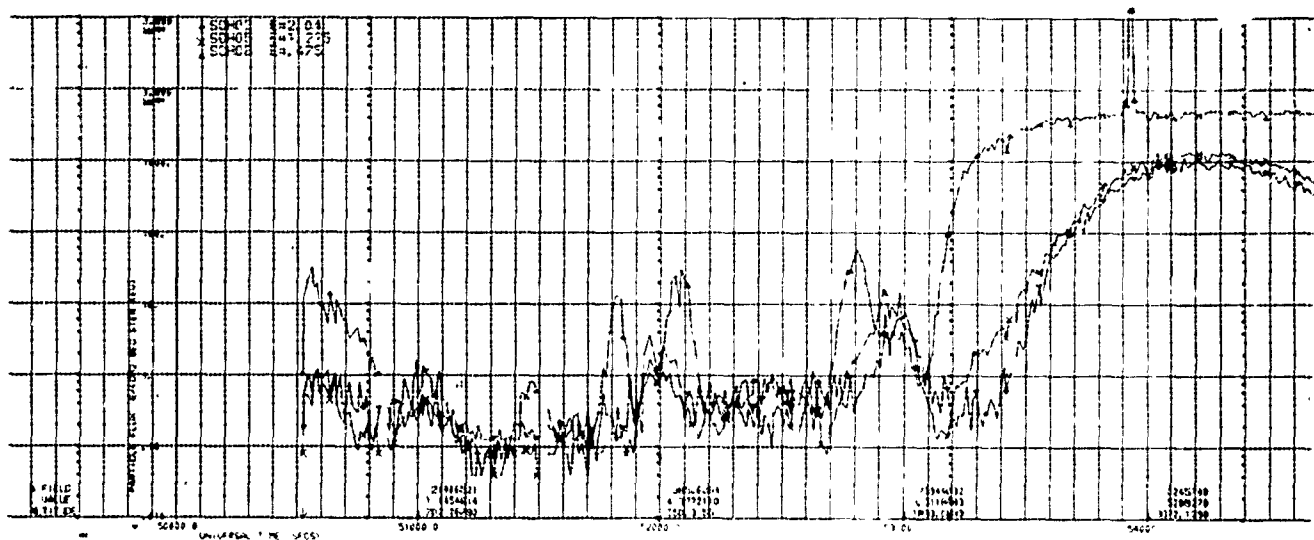
The character of the data virtually dictated a statistical approach. The data was taken at different altitudes, local times, and conditions of magnetic activity. In addition, coverage was such that in few cases are there two consecutive revolutions of data, and even two cutoffs taken under similar conditions are few. In most cases the data was separated by days and conditions varied accordingly. It was thus impossible to relate the changes of cutoffs over an extended period of time to the changing conditions.

The local time referred to in this study is the geographic local time of the point where the cutoff was observed. The expression used

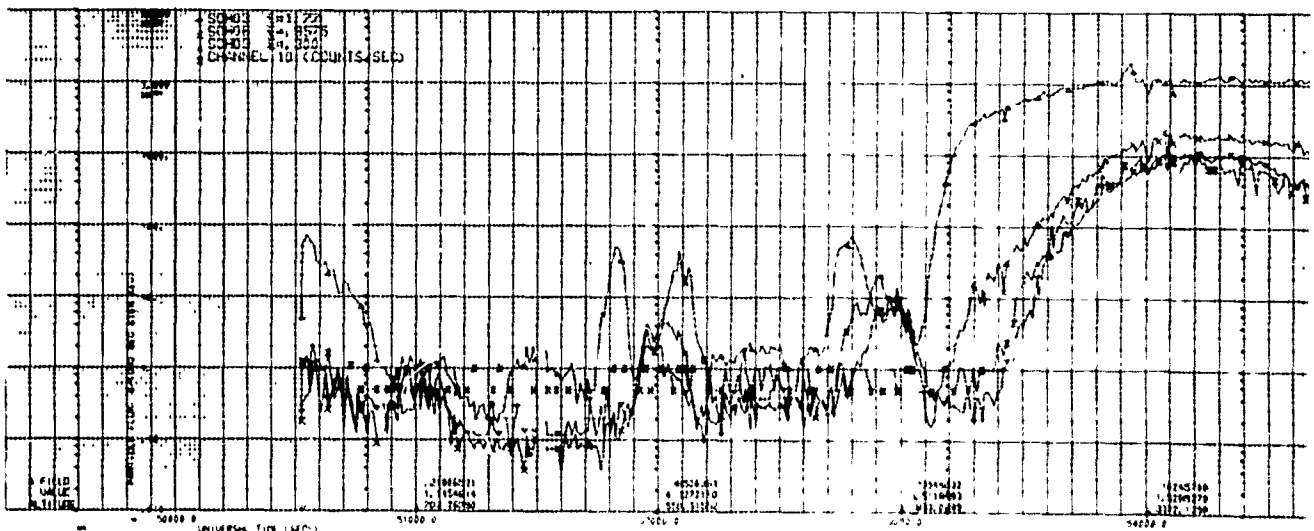
**CHANNELS 1, 4, 7**



**CHANNELS 2, 5, 8**



**CHANNELS 3, 6, 9**



PERIGEE  
(ATMOSPHERIC  
CUTOFF)

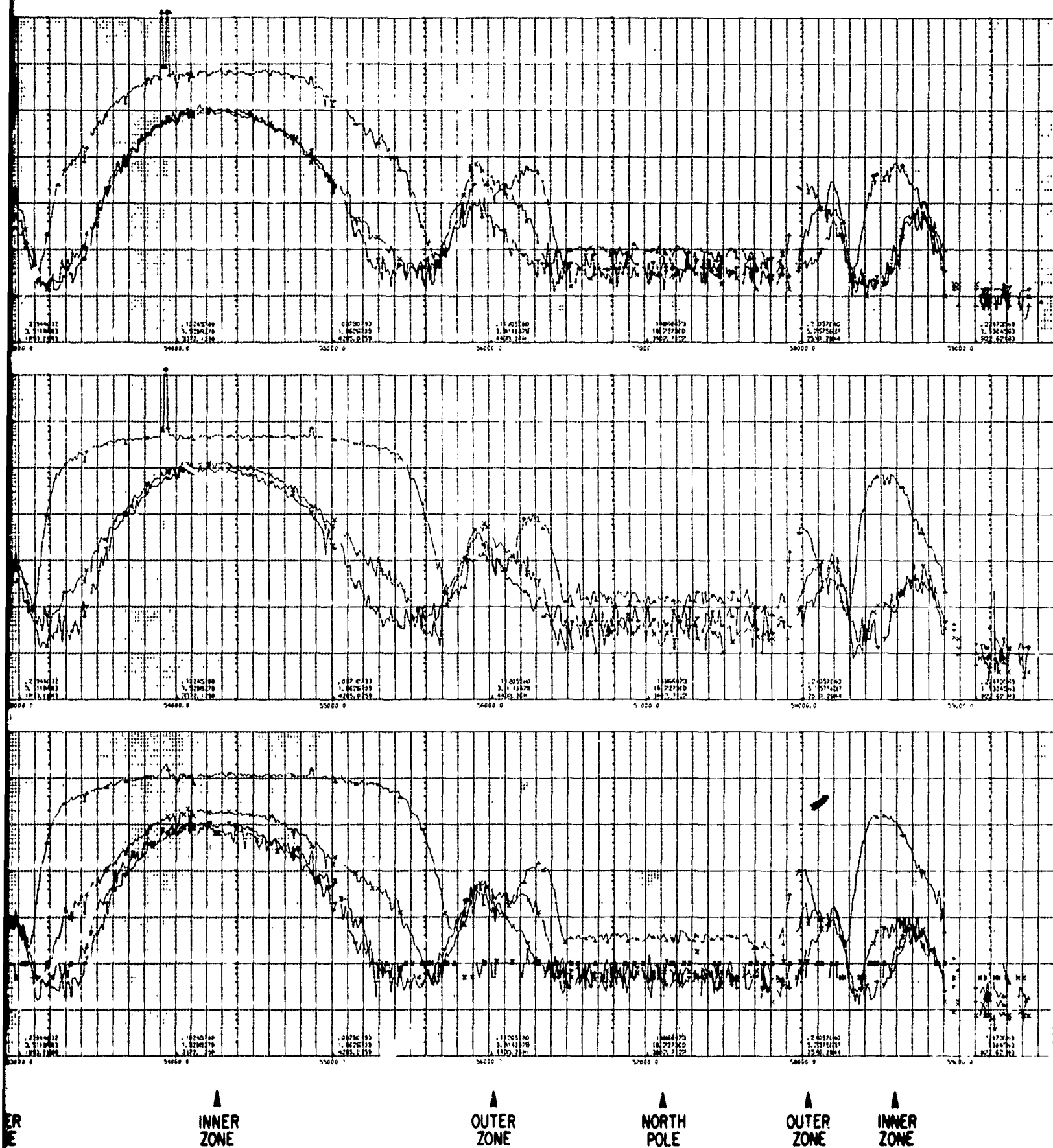
**A  
OUTER  
ZONE**

**A  
OUTER  
ZONE**

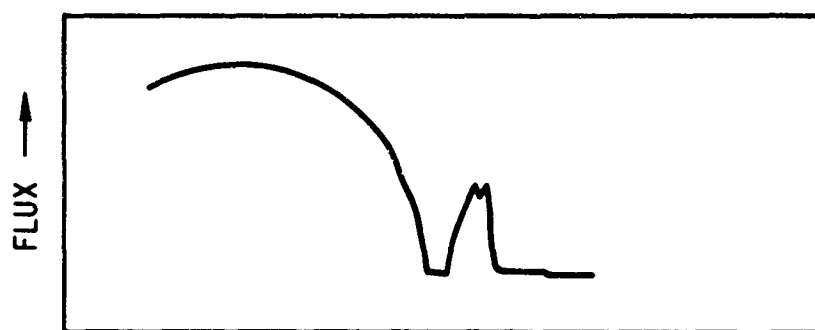
**INNER  
ZONE**

FIG. 11. PLOT OF  $J_1$  versus UNIVERSAL TIME FOR SHOWS SOLAR FLARE ELECTRONS

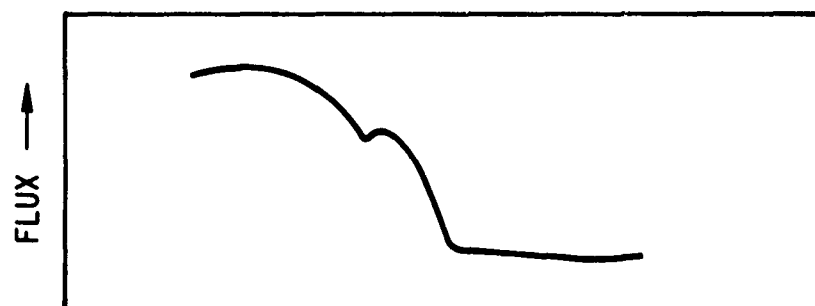
A



F<sub>1</sub> versus UNIVERSAL TIME FOR REV 1926, FEBRUARY 3, 1967 WHICH  
POLAR FLARE ELECTRONS



UNIVERSAL TIME →  
*(a) DEFINITE SPIKE.*



UNIVERSAL TIME →  
*(b) POSSIBLE ENCLOSED SPIKE.*



UNIVERSAL TIME →  
*(c) CUTOFF PUSHED OUT POSSIBLY  
DUE TO SPIKE OR MULTIPLE  
SPIKES.*

FIG. 12. TYPES OF SPIKE PHENOMENON OBSERVED DURING MAGNETICALLY  
DISTURBED PERIODS

TABLE I: Data on High Latitude Spikes

<u>Day of Observation</u>	<u>Local Time (hours)</u>	<u>Type of Observation</u>
235	1415	definite spike
249	2128	" "
250	0808	evidence of a spike
251	1049	" " "
251	1013	" " "
251	2246	definite spike
252	1304	evidence of a spike
252	2105	definite spike
252	0731	evidence of a spike
253	0730	" " "
259	0944	" " "
271	2214	" " "
271	0551	" " "
271	0014	definite spike
273	0605	evidence of a spike
273	0645	" " "
277	2250	" " "
297	0930	definite spike
339	0145	" "
339	0546	evidence of a spike

in its calculation is

$$LT = UT/3600 + E/15 \quad (2)$$

where LT is the local time in hours, UT is the universal time in seconds and E is the east longitude in degrees. Probably a more correct parameter would have been magnetic local time. However, due to the time and effort required to obtain this parameter, geographic local time was used instead. McDiarmid (private communication) stated that, in his study of cutoffs, he found little difference between magnetic and geographic local times.

From the data on cards, initial plots were made of cutoffs versus altitude, local time, and the 3 hr  $K_p$  averages. Each energy for each pole was plotted separately. Although there was a good deal of scattering of the points, it was clear that for the statistical approach being used the North Pole and South Pole data could be superimposed. This was not unexpected since the magnetospheric model used by the computer for data reduction corrected for the north-south asymmetry of the magnetosphere.

This superposition yielded about double the density of data points to work with. Running these plots off again for each energy still left the scattering problem apparent in the initial plots. Examples of the three types of plots appear as Figures 13 through 15. Since variations in magnetic activity should be approximately random, relations to remove the altitude and local time dependences were sought.

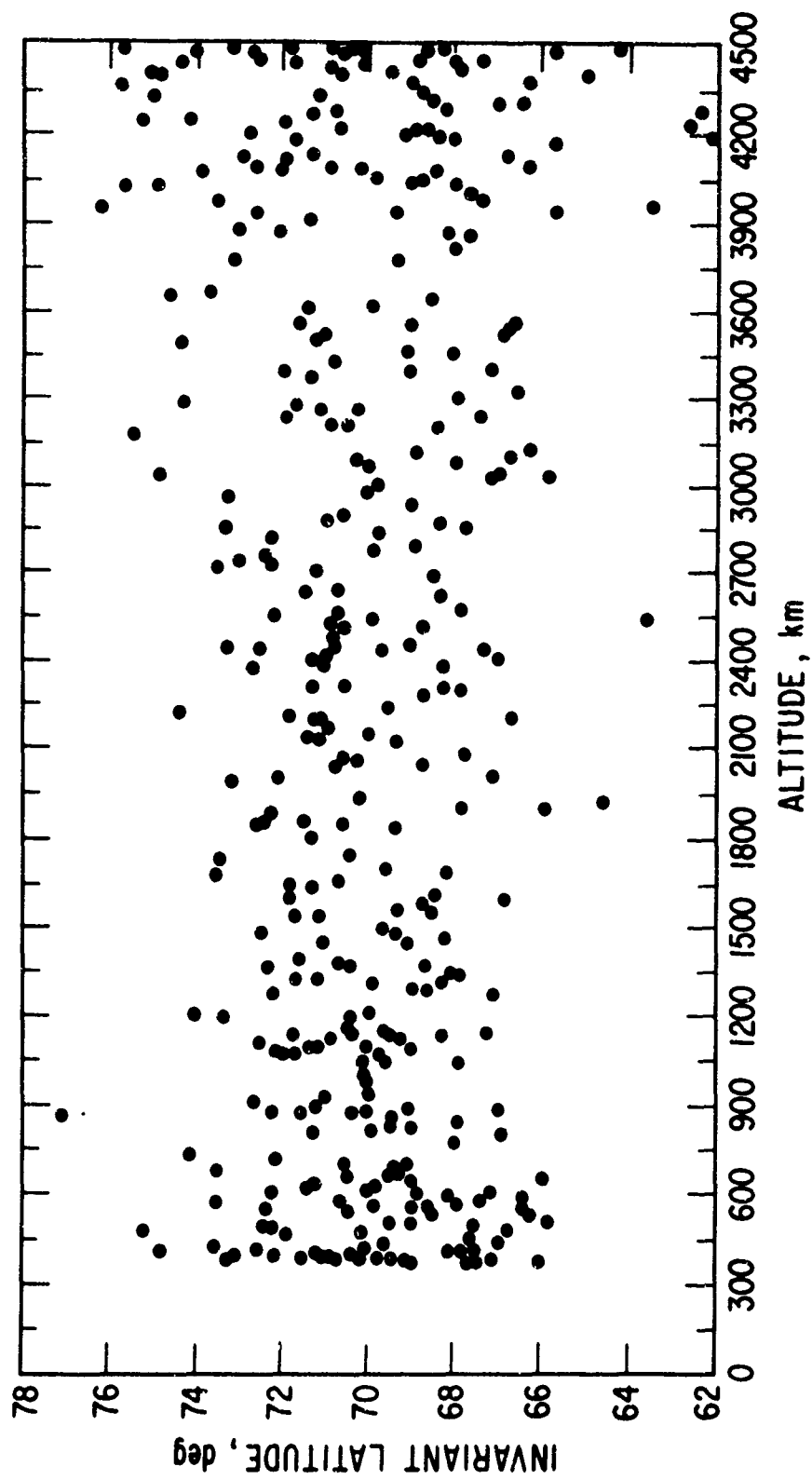


FIG. 13. PLOT OF CUTOFF versus ALTITUDE FOR CHANNEL 7



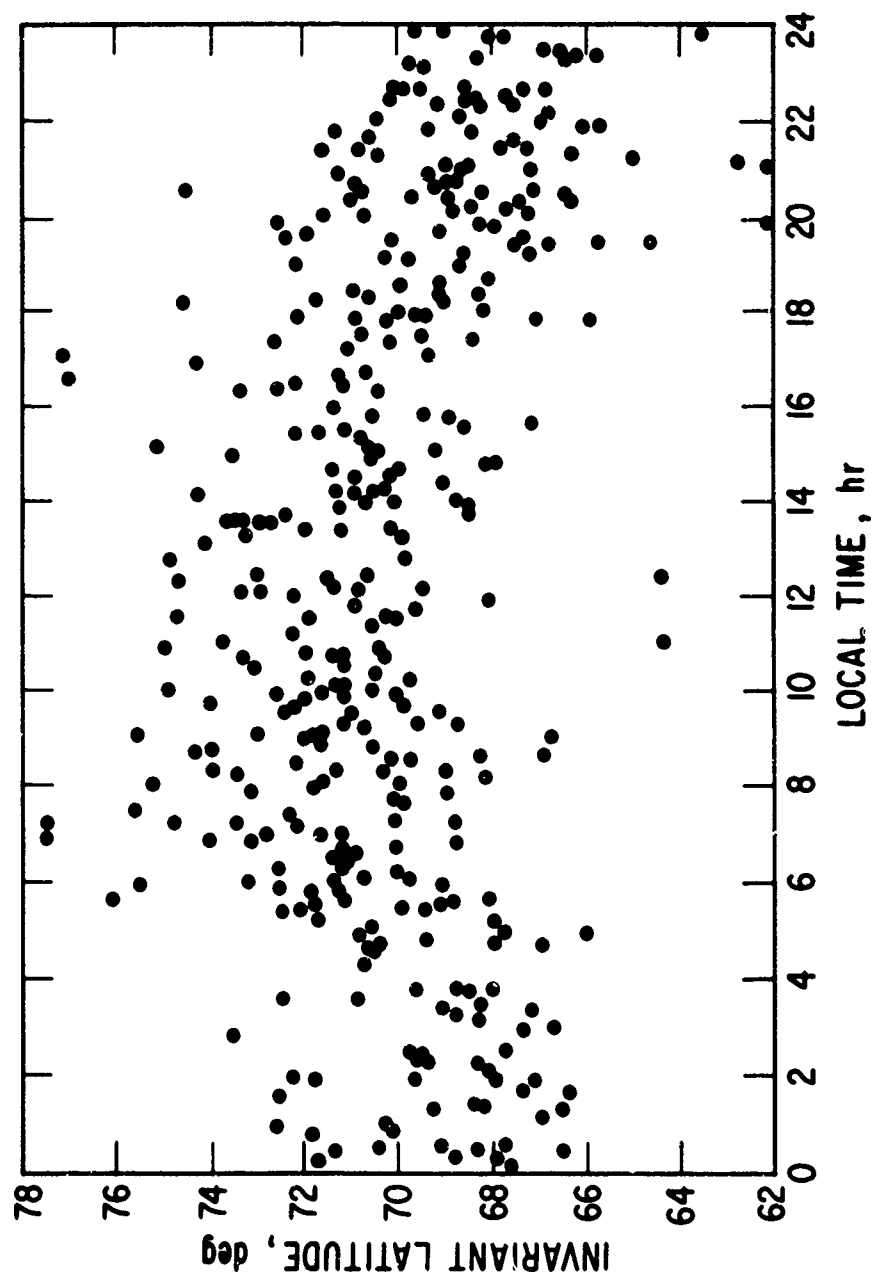


FIG. 14. PLOT OF CUTOFF versus LOCAL TIME FOR CHANNEL 7

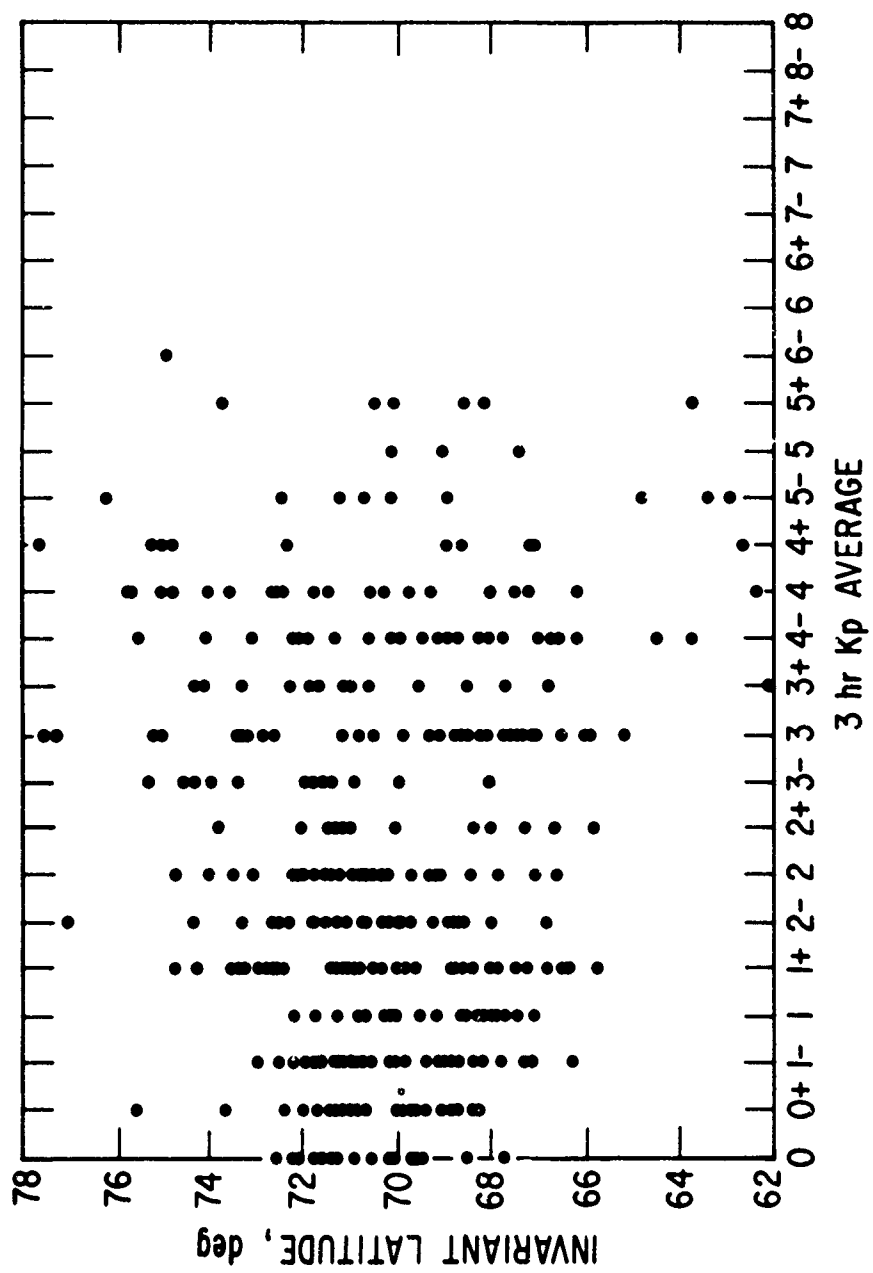


FIG. 15. PLOT OF CUTOFF versus THE 3HR AVERAGE Kp INDEX FOR CHANNEL 8

An examination of the nine plots of  $\Lambda$  versus altitude indicated that the cutoffs were independent of altitude in this experiment. In none of the nine cases did any trend seem to be indicated. If any trend were really present, it should at least be detectable in these plots.

The initial plots made it clear that there was a local time dependence. Half-hour averages and the associated standard deviations were computed and plotted. This was done to eliminate any confusion caused by the varying density of points over local time and to prevent biasing of any attempted fits to the data. As shown in Figure 16, the scattering still existed, although a definite trend was visible. A fourth order fit to this average data failed to merge smoothly around the endpoints. Thus, the average values from 0 to 24 hr were reproduced from 24 to 48 hr and a ninth order fit was found satisfactory, as shown in Figure 17. Then a fourth order fit to this ninth order curve over the range from 12 to 36 hr was made. The final result obtained was

$$\begin{aligned} \Lambda_i &= \sum_{j=1}^5 C_{ij} (T+24)^{j-1} & 0 \leq T \leq 12 \\ \Lambda_i &= \sum_{j=1}^5 C_{ij} T^{j-1} & 12 \leq T \leq 24 \end{aligned} \quad (3)$$

where  $i$  is the channel number,  $T$  is the local time in hours,  $\Lambda$  is the cutoff in degrees, and  $C$  is the appropriate coefficient determined from the fourth order fit. Channels 2 through 9 yielded satisfactory

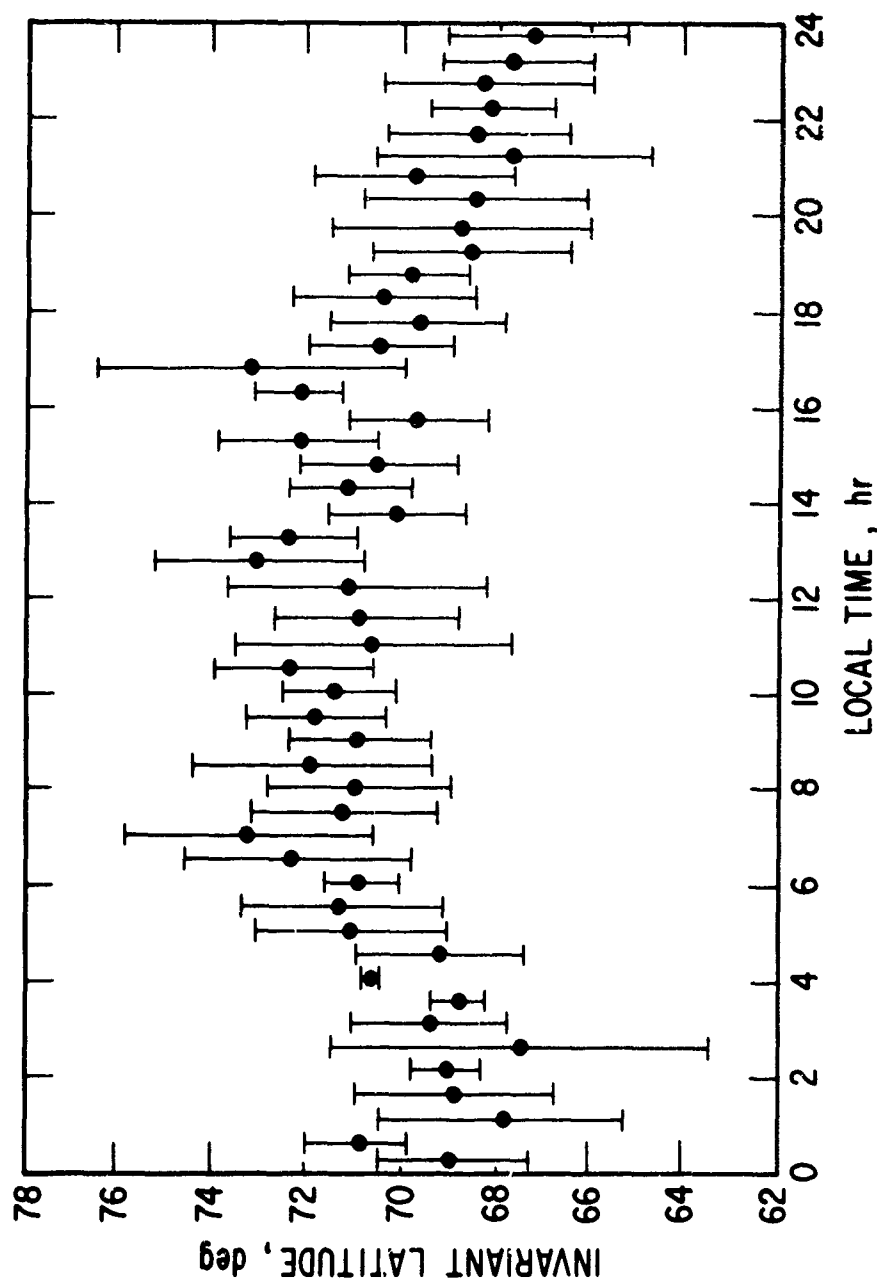


FIG. 16. PLOT OF CUTOFFS AVERAGED OVER HALF HOUR INTERVALS AND ASSOCIATED STANDARD DEVIATIONS AS A FUNCTION OF LOCAL TIME FOR CHANNEL 8

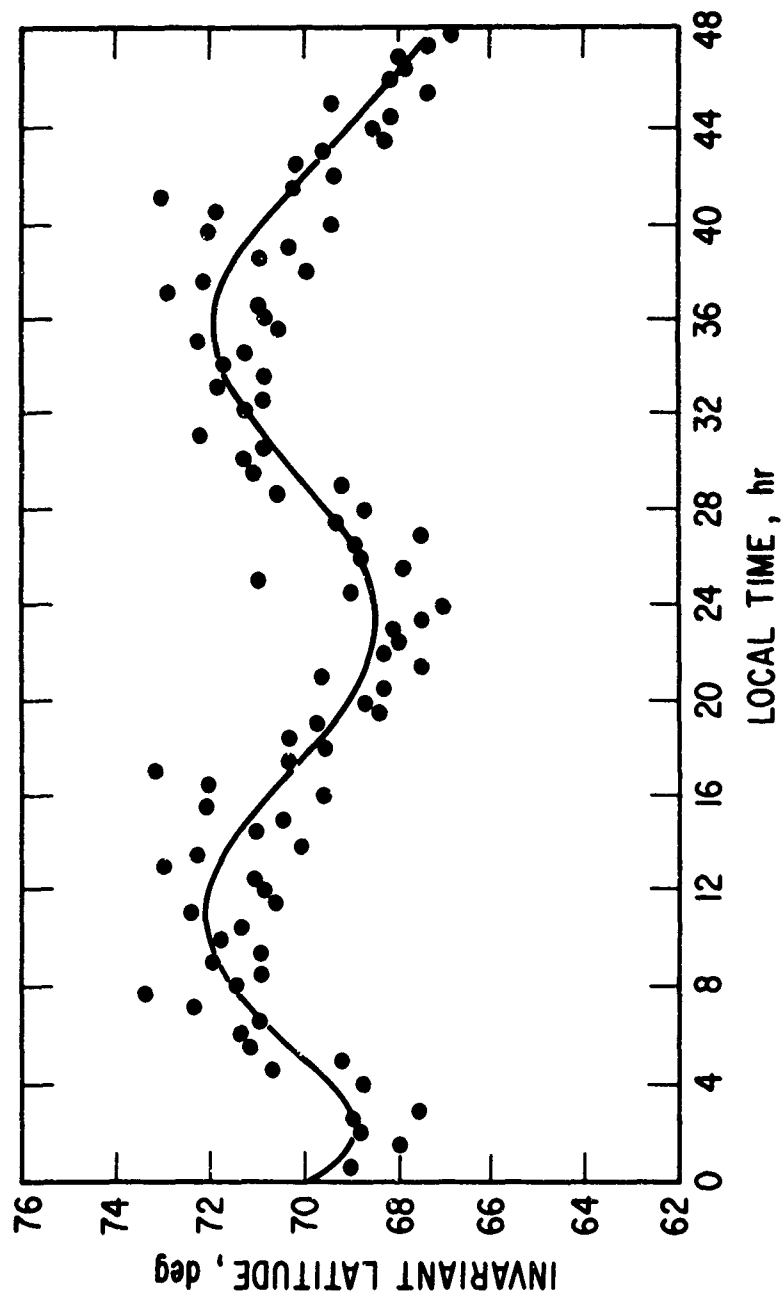


FIG. 17. NINTH ORDER FIT TO THE AVERAGE CUTOFF versus LOCAL TIME PLOT  
REDUNDANTLY EXTENDED OVER 48 HOURS.

results from this fitting process. The values of the coefficients appear in Table II. The Channel 1 fit, however, became physically unrealistic probably because of the few data points, large deviations and small diurnal variation. The Channel 8 fit is shown in Figure 18.

Several distinct features show up in Figure 19, which shows all eight fits together. The local time plots for all the energies seem to have maxima around 1100 hr local time and minima around 2300 hr. The plots seem approximately symmetrical with respect to the 1100-2300 hr meridian and show a diurnal variation, which decreases with increasing energy. The higher energy electrons cut off at lower latitudes for all local times; the spread of cutoffs is largest around 1100 and smallest around 2300 hr. In general, the cutoffs agreed well with those reported by others.

Since the diurnal variation appeared to be a function of energy, plots of  $\Delta A$  as a function of  $\Lambda_{MAX}$ ,  $\Lambda_{MIN}$ , and  $\Lambda_{AVG}$  were run off for matched passes over the poles. More specifically the values were obtained using only two data points taken over the same pole on the same revolution. This was designed to determine whether the diurnal variation was actually a function of energy or a function of the magnetic field configuration where the energies involved characterize different L shells. Williams and Mead reported a correlation between the day-side cutoffs and the magnitude of the diurnal variation for matched pass data in 1965 (Ref. 16:3021). All available matched pass data from the present study was plotted and each pair of points grouped

TABLE II.

COEFFICIENTS FOR THE EXPRESSION OF THE CUTOFF AS A FUNCTION OF LOCAL TIME

Channel Number, i	$C_{i1} \times 10^{-1}$	$C_{i2}$	$C_{i3} \times 10$	$C_{i4} \times 10^3$	$C_{i5} \times 10^5$
2	6.1566441	1.4586307	-1.2554237	4.1363753	-4.6106446
3	6.4503926	1.0846253	-1.1005931	4.0034746	-4.7825338
4	6.2975231	1.6829297	-1.6038332	5.6191813	-6.5296576
5	5.5140188	3.3765577	-2.7757116	8.9124553	-9.7592165
6	5.4527357	3.7191320	-3.0679784	9.8528584	-10.776861
7	4.9464471	5.1252472	-4.1821950	13.358259	-14.571569
8	4.5278151	6.3282272	-5.1210093	16.286748	-17.707935
9	4.3266078	7.3051118	-6.0816939	19.761451	-21.878785

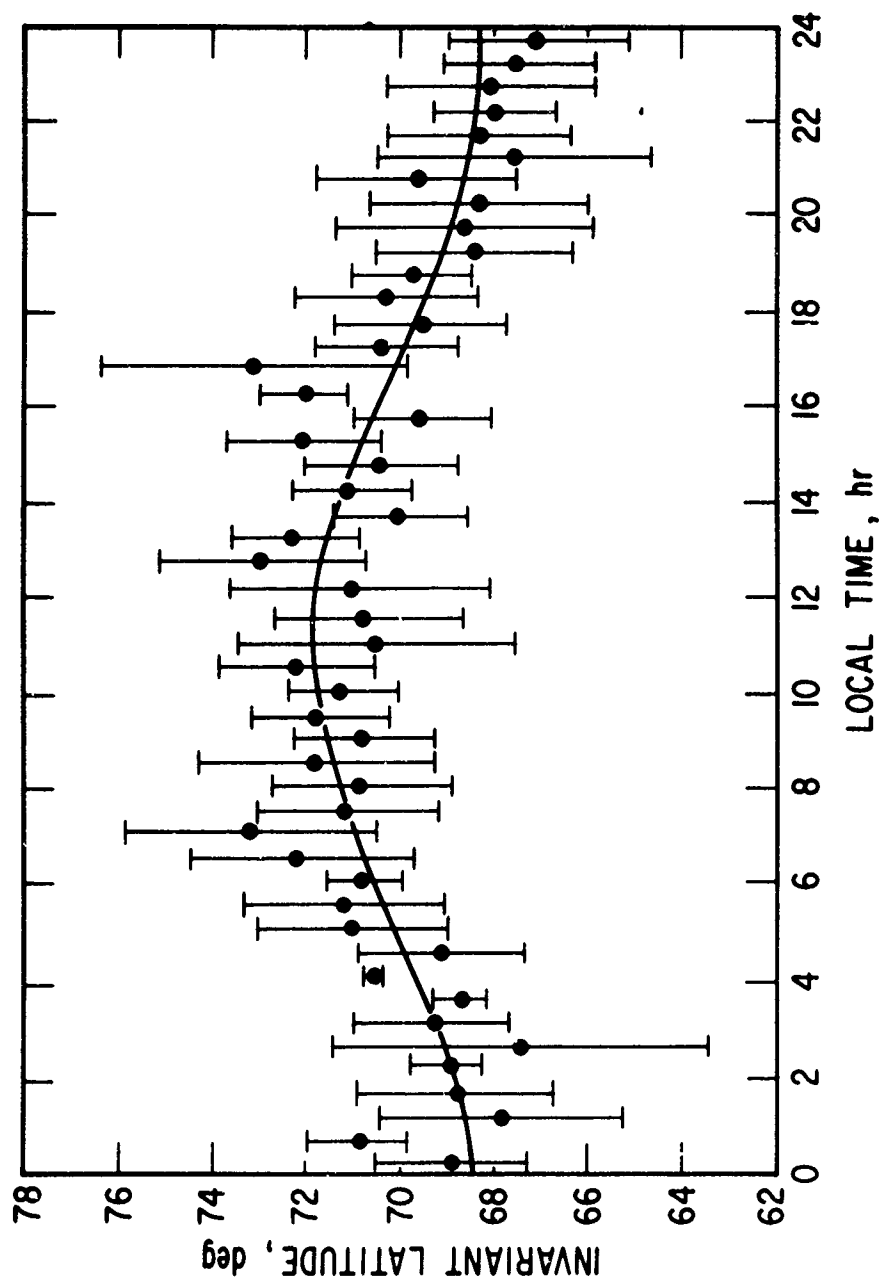


FIG. 18. FOURTH ORDER FIT TO NINTH ORDER CURVE OVER THE INTERVAL 12 TO 36 HOURS CORRECTED  $\delta^*_{\text{SK}}$  TO 0 TO 24 HOURS AND COMPARED WITH DATA



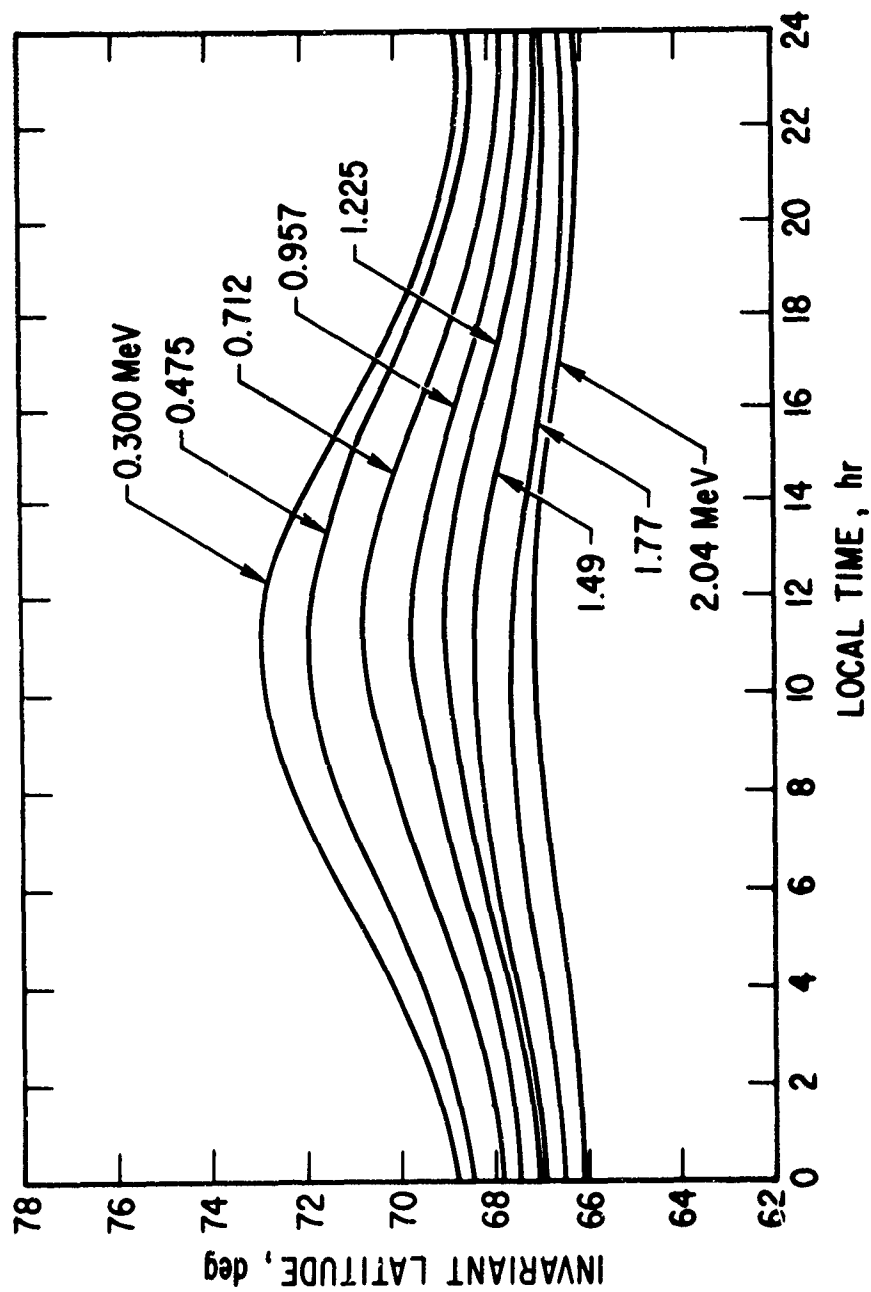


FIG. 19. PLOT OF EMPIRICAL FITS TO THE CUTOFF versus LOCAL TIME PLOTS FOR CHANNELS 2 THROUGH 9

into a 2-hr interval according to the earlier local time. For example, two points with local times of 0200 and 1400 hr would fall into the 0000-0200 interval. The two local times sampled, however, were usually somewhat less than 12 hr apart. In most cases the two times were 6 to 10.5 hr apart.

Many of the plots had too few points to indicate any definite trends, but examples of some of the more successful plots appear in Figures 20 through 22. The plots of  $\Delta\Lambda$  versus  $\Lambda_{\text{MIN}}$  show little but those of  $\Delta\Lambda$  versus  $\Lambda_{\text{MAX}}$  show most points falling below a curve with a positive slope and an X intercept, which varies inversely as the energy. One would expect points to fall below such a curve, since the points represent data with varying local time differences, the higher points having differences closer to the maximum of 12. The  $\Delta\Lambda$  versus  $\Lambda_{\text{AVG}}$  plots were similar to those of  $\Delta\Lambda$  versus  $\Lambda_{\text{MAX}}$ , but they had a greater slope and lower X intercept.

The results of these observations are inconclusive. One would expect the positive  $\Lambda_{\text{MAX}}$  slope because  $\Delta\Lambda$  is dependent directly on  $\Lambda_{\text{MAX}}$  and  $\Lambda_{\text{MIN}}$ . The intercept variation may be due to the difference between the two local times sampled on each matched pass, which varies according to energy or to where the cutoff occurred. Since the higher energy cutoffs occur at lower latitudes, the two times sampled are usually farther apart. Thus, one would expect the higher energy curves to fall above those of the lower energies, as is the case.

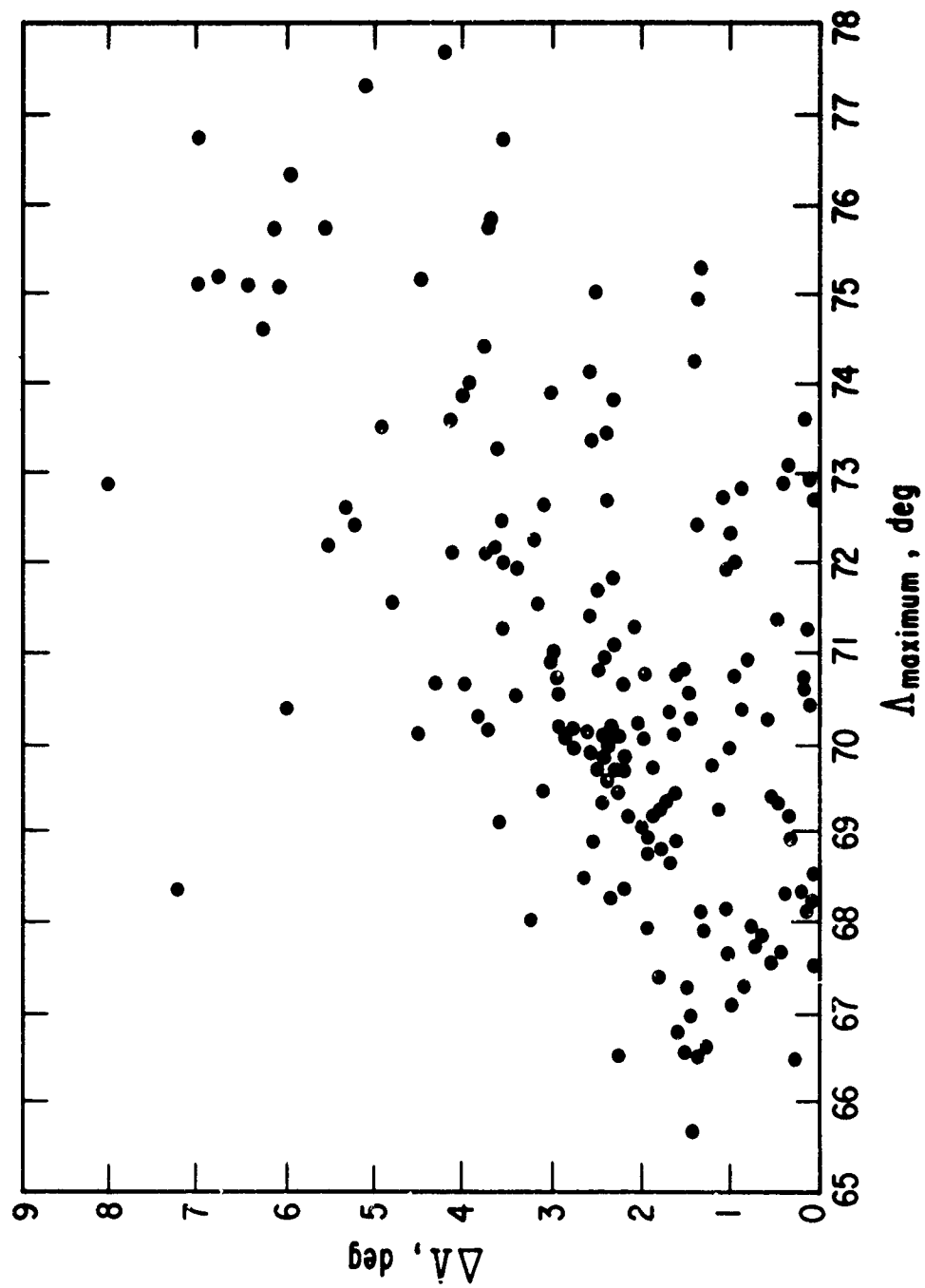


FIG. 20. PLOT OF DIURNAL VARIATION OF CUTOFF AS A FUNCTION OF THE HIGHER CUTOFF FOR MATCHED PASS DATA FROM ALL CHANNELS WITH ONE DATA POINT FALLING IN THE LOCAL TIME INTERVAL OF 0000-0200 HOURS

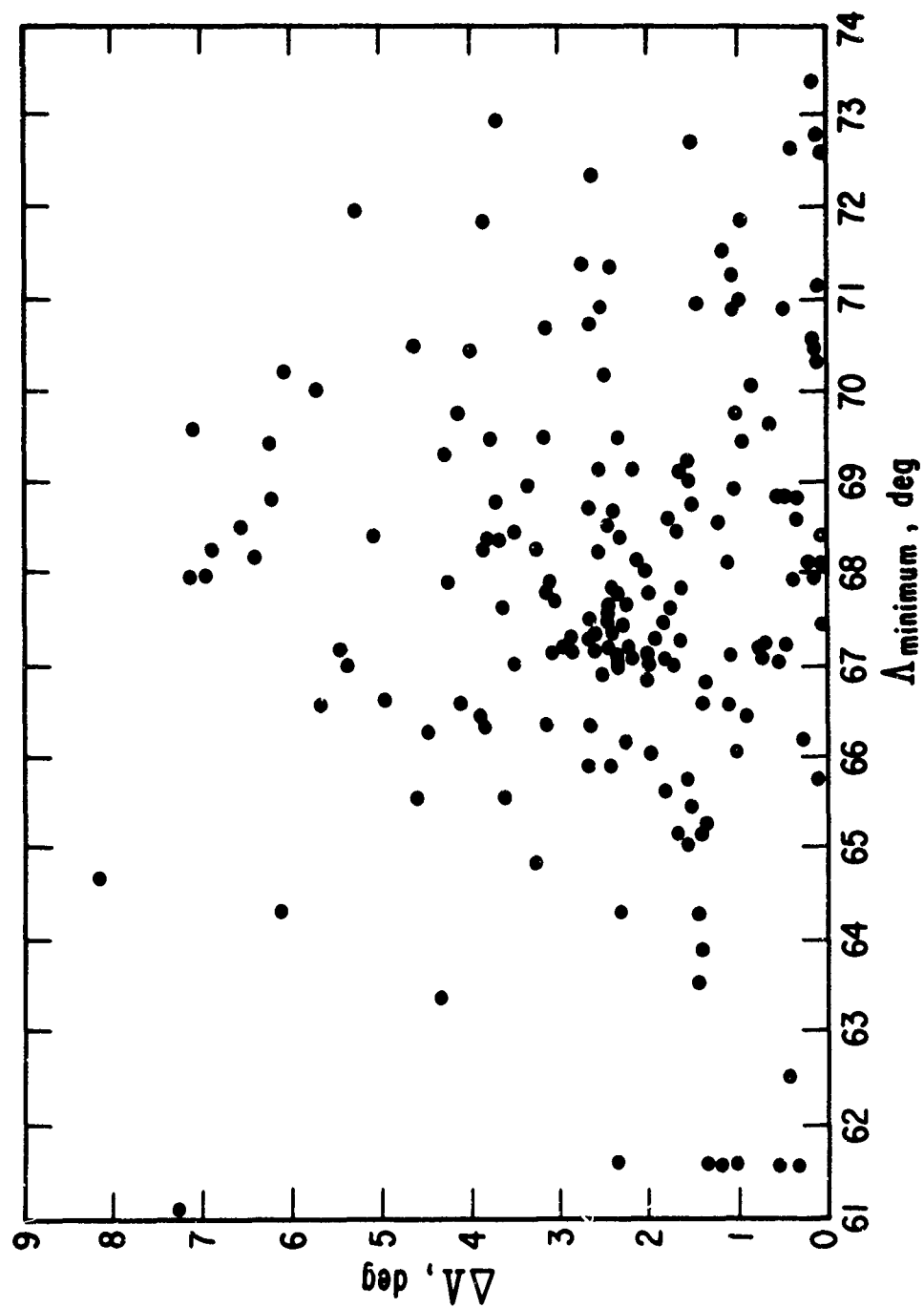


FIG. 21. PLOT OF DIURNAL VARIATION OF CUTOFF AS A FUNCTION OF THE LOWER CUTOFF FOR MATCHED PASS DATA FROM ALL CHANNELS WITH ONE DATA POINT FALLING IN THE LOCAL TIME INTERVAL OF 0000-0200 HOURS

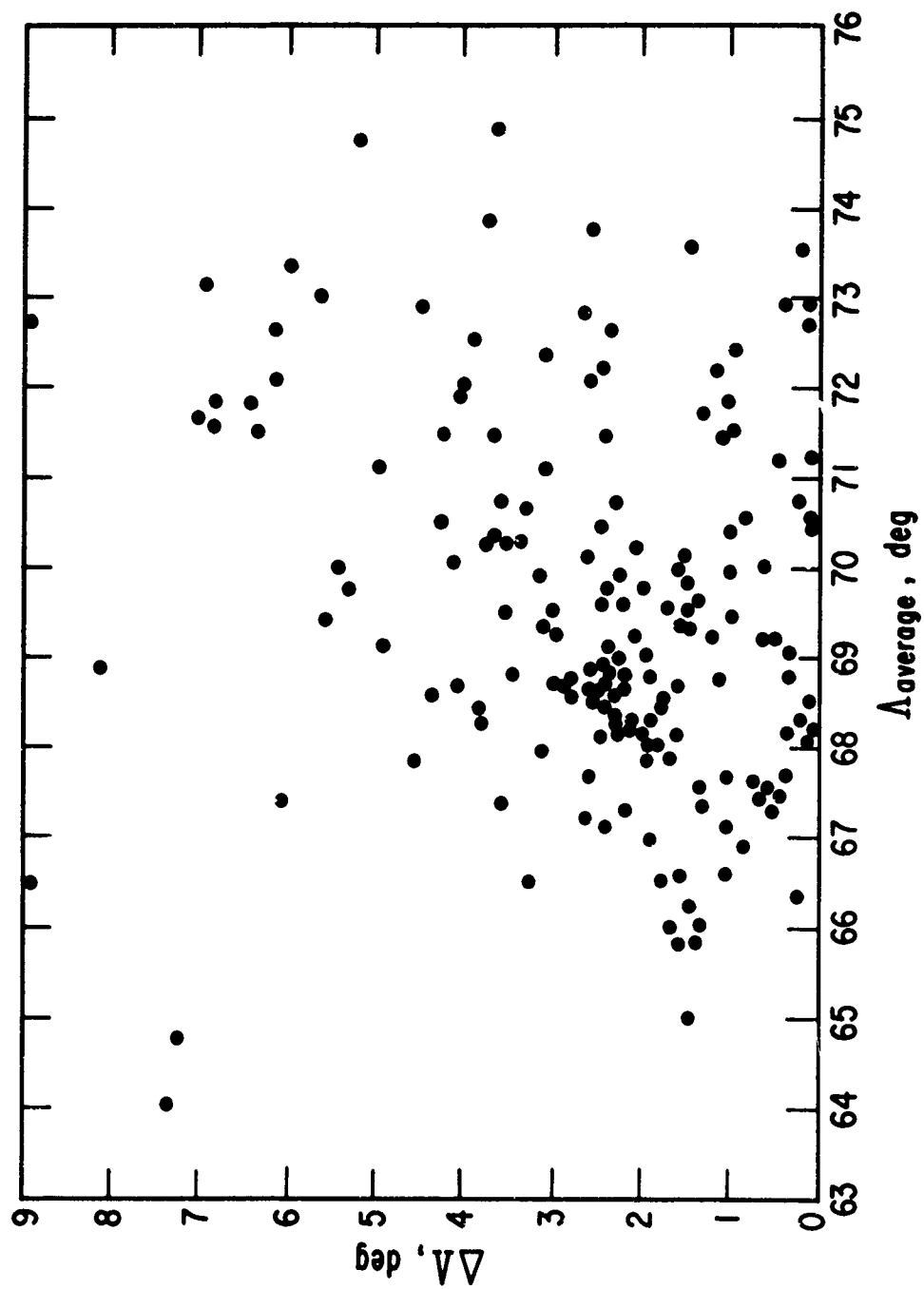


FIG. 22. PLOT OF DIURNAL VARIATION OF CUTOFF AS A FUNCTION OF THE AVERAGE CUTOFF FOR MATCHED PASS DATA FROM ALL CHANNELS WITH ONE DATA POINT FALLING IN THE LOCAL TIME INTERVAL OF 0000-0200 HOURS

The  $\Lambda_{AVG}$  plots would be expected to fall somewhere between the  $\Lambda_{MIN}$  and  $\Lambda_{MAX}$  results, and, as far as the data indicates, this does occur.

The effect of the variation of local time differences with energy could be eliminated by application of a selection criterion to the points before plotting. This was tried in two ways. Requiring a time difference of between 10 and 12 hr reduced the number of usable data points so drastically that the plots were virtually useless, while requiring a difference between 9 and 12 hr yielded essentially the same results as those obtained with no selection.

With the previously obtained expressions for the cutoff as a function of local time, the data for Channels 2 through 8 were normalized to 68 deg and replotted as a function of the 3-hr average  $K_p$  indices, as shown in Figure 23. The plots were made with varying time lags. For example,  $\Lambda$  was plotted as a function of the  $K_p$  value within which the observation was taken, the  $K_p$  value preceding the one during the observation, and so on. The only trend detected was that the spread of cutoffs was greatest during times of higher  $K_p$  values. To be sure nothing was being masked by the scattering of the data, average values of the cutoffs were calculated and plotted over intervals of  $K_p$ . As shown in Figure 24, nothing new became apparent.

In 1968, Williams, Arens, and Lanzerotti found an excellent correlation between the appearance of energetic electrons during

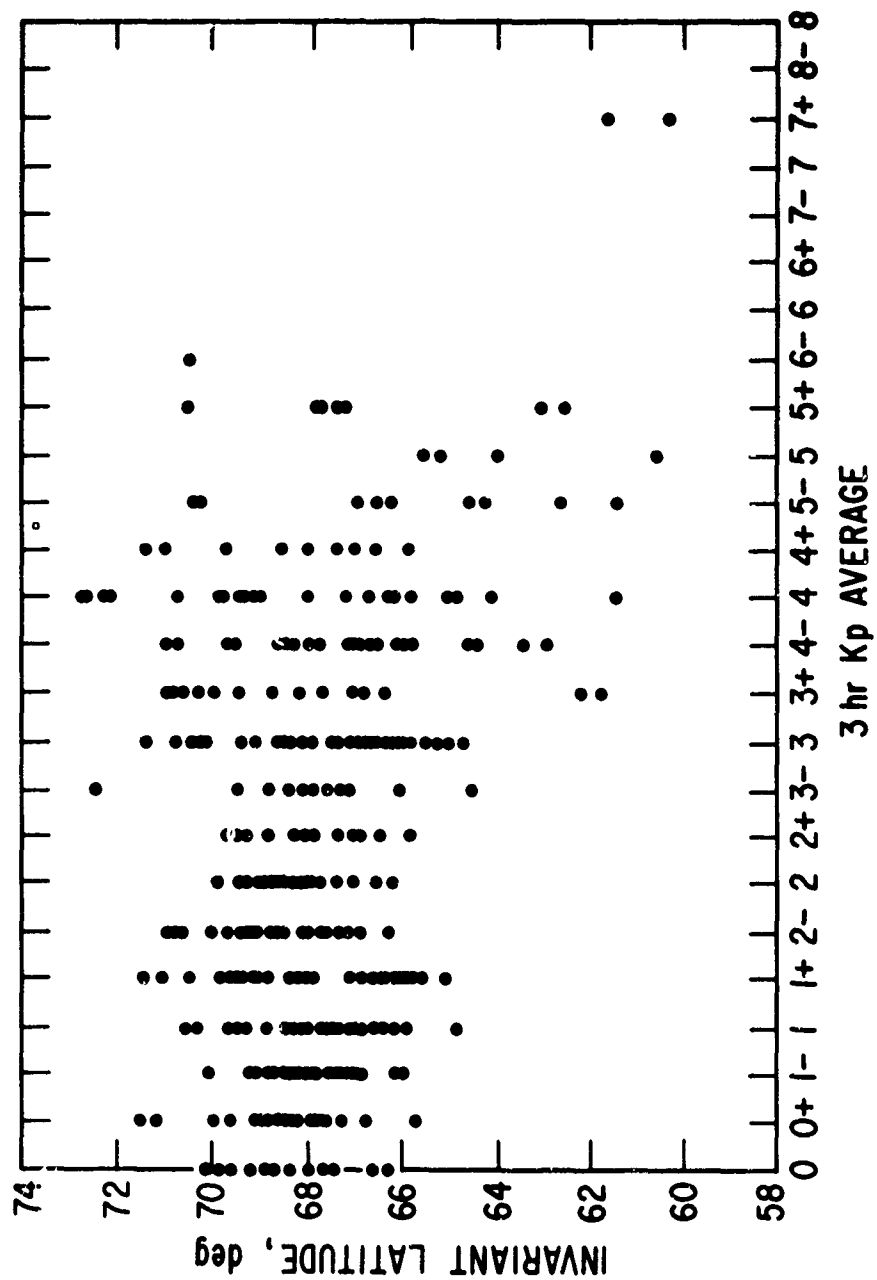


FIG. 23. PLOT OF LOCAL TIME CORRECTED CUTOFF versus THE 3 HOUR AVERAGE Kp INDEX FOR CHANNEL 7 WITH NO TIME LAG

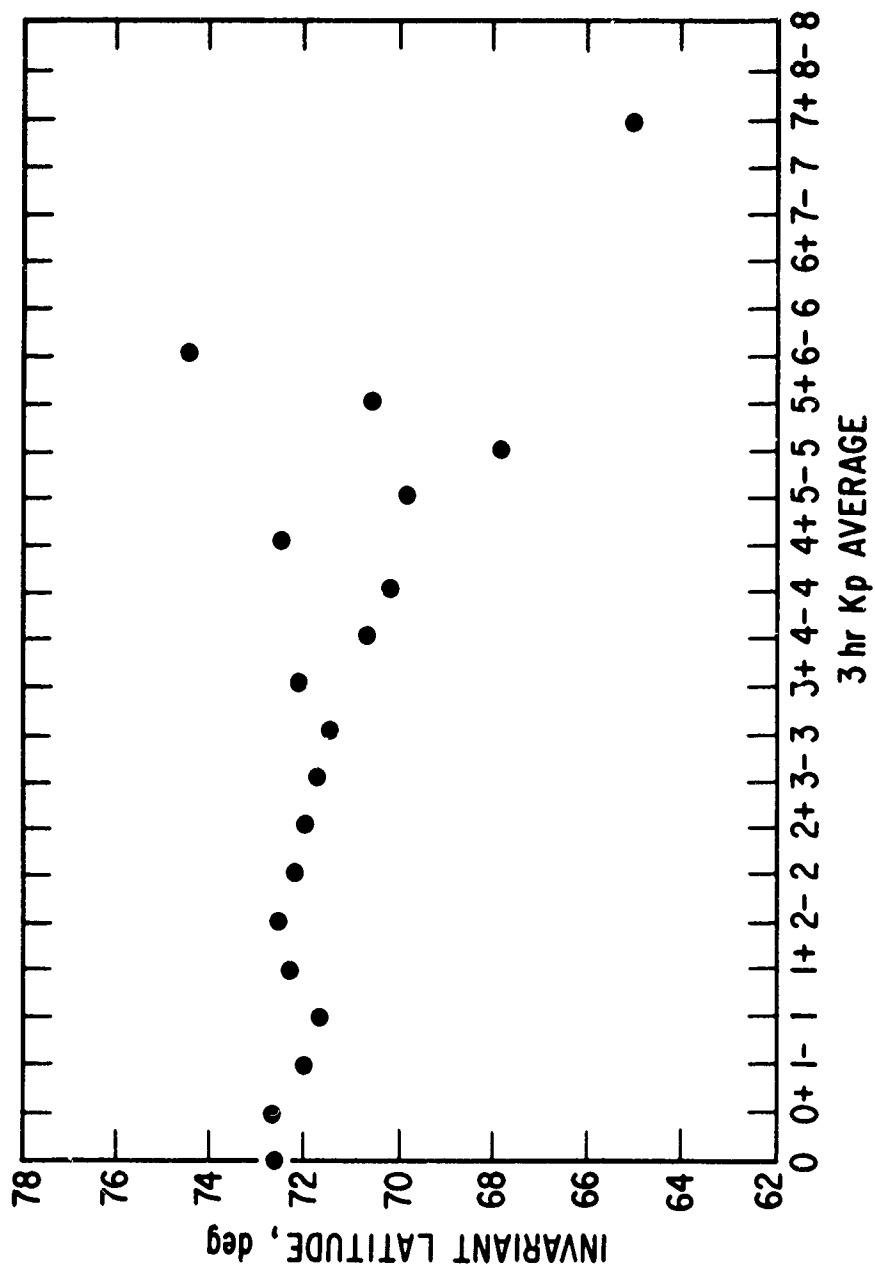


FIG. 24. PLOT OF LOCAL TIME CORRECTED CUTOFFS AVERAGED OVER  $K_p$  INCRIMENTS AS A FUNCTION OF THE 3HR AVERAGE  $K_p$  INDEX FOR CHANNEL 7 WITH NO TIME LAG



storms and Dst (Ref. 17:5673). After finding no correlation between  $K_p$  and the cutoffs, Dst was tried. Dst is a measure of the magnetic field produced by currents flowing at great distances from the earth and is often associated with ring current measurements. Magnetic storms produce large negative Dst values (Ref. 10:40). Hourly values of Dst were obtained through the courtesy of Drs. M Suguira and S. Hendricks enabling plots of  $\Lambda$  versus Dst to be run off. The cutoffs were corrected for local time, and the plots were made for Dst values from 5 hr before the cutoff was observed to 5 hr after. One of the plots appears in Figure 25. The bunching of points made these initial plots difficult to interpret, so the cutoffs were averaged over intervals of Dst and replotted, as shown in Figure 26.

For Dst values from -35 to +25 gamma, where the density of points is high enough to make the averages meaningful, no trends are visible, as can be seen in Figure 26 which can be considered representative of the other Channel 9 plots. In the region below -35 gamma, where there are few points, the average values seem to tail off. This is also true of the other plots. Figure 27 shows the averages for all 10 of the correlations for Dst values from 5 hr before to 5 hr after the observation. Figure 27 is for the Channel 9 data but the other channels behaved in essentially the same way.

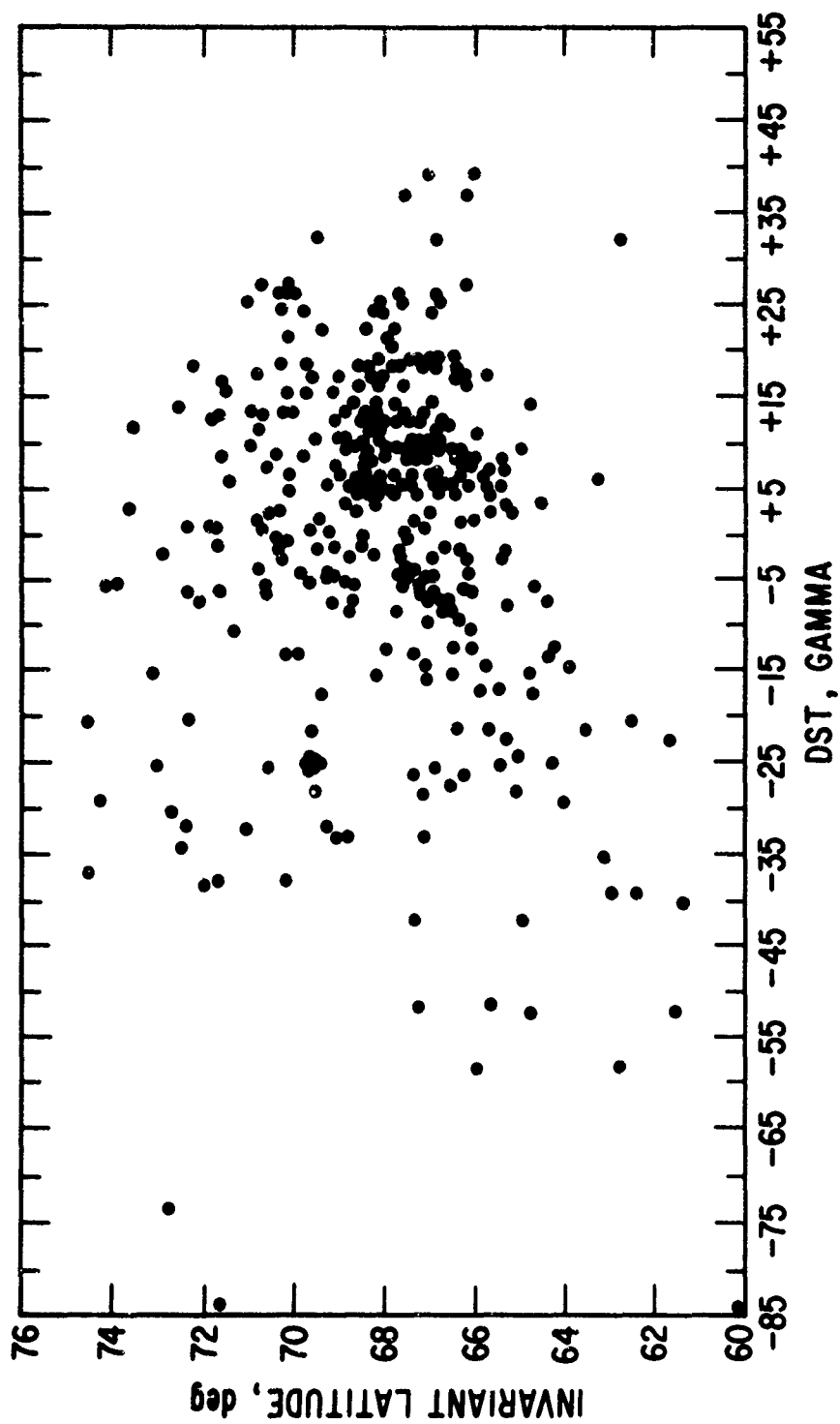


FIG. 25. PLOT OF LOCAL TIME CORRECTED CUTOFF versus DST FOR CHANNEL 9 WITH NO TIME LAG

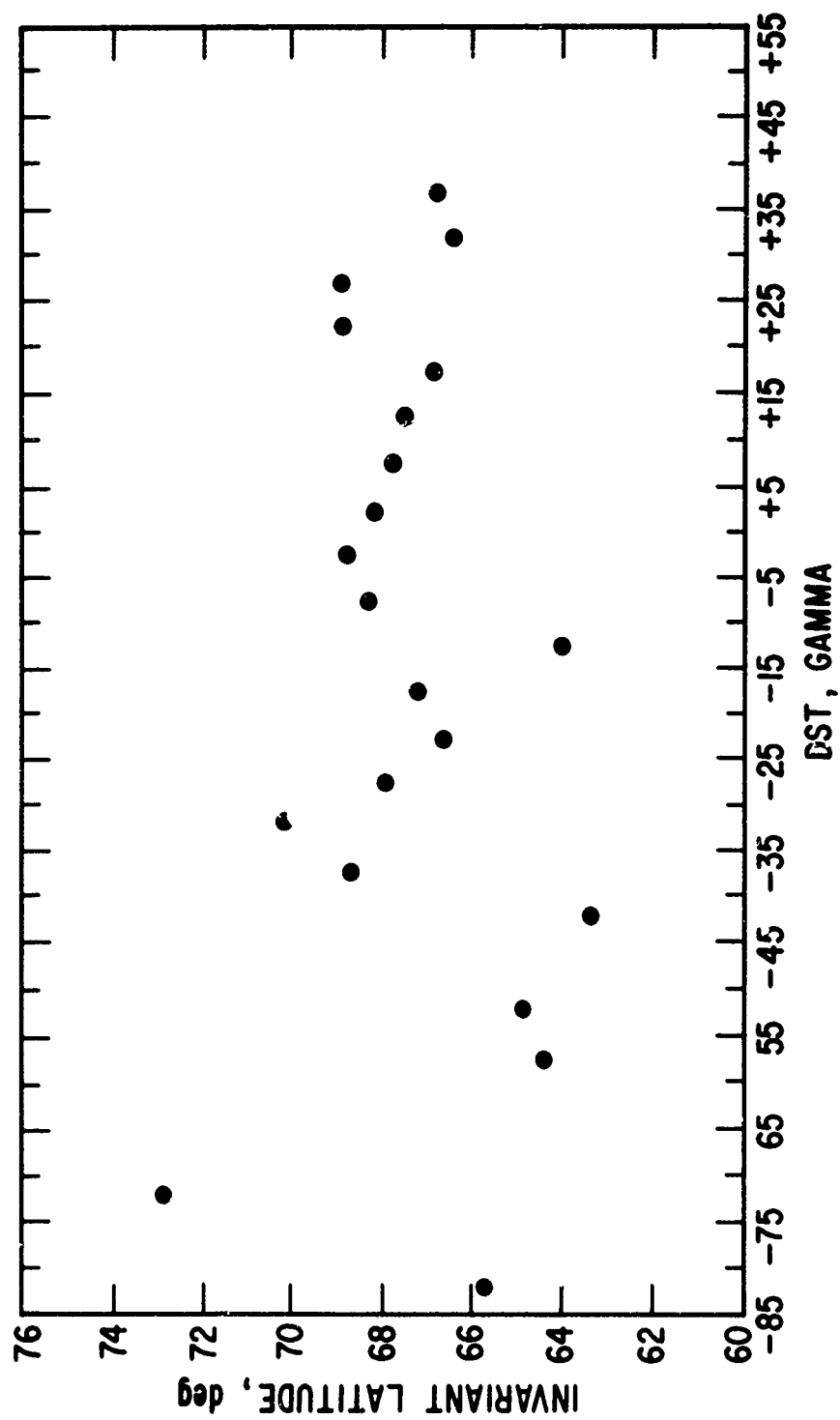


FIG. 26. PLOT OF LOCAL TIME CORRECTED CUTOFFS AVERAGED OVER 5 GAMMA INTERVALS VERSUS DST FOR CHANNEL 9 WITH NO TIME LAG

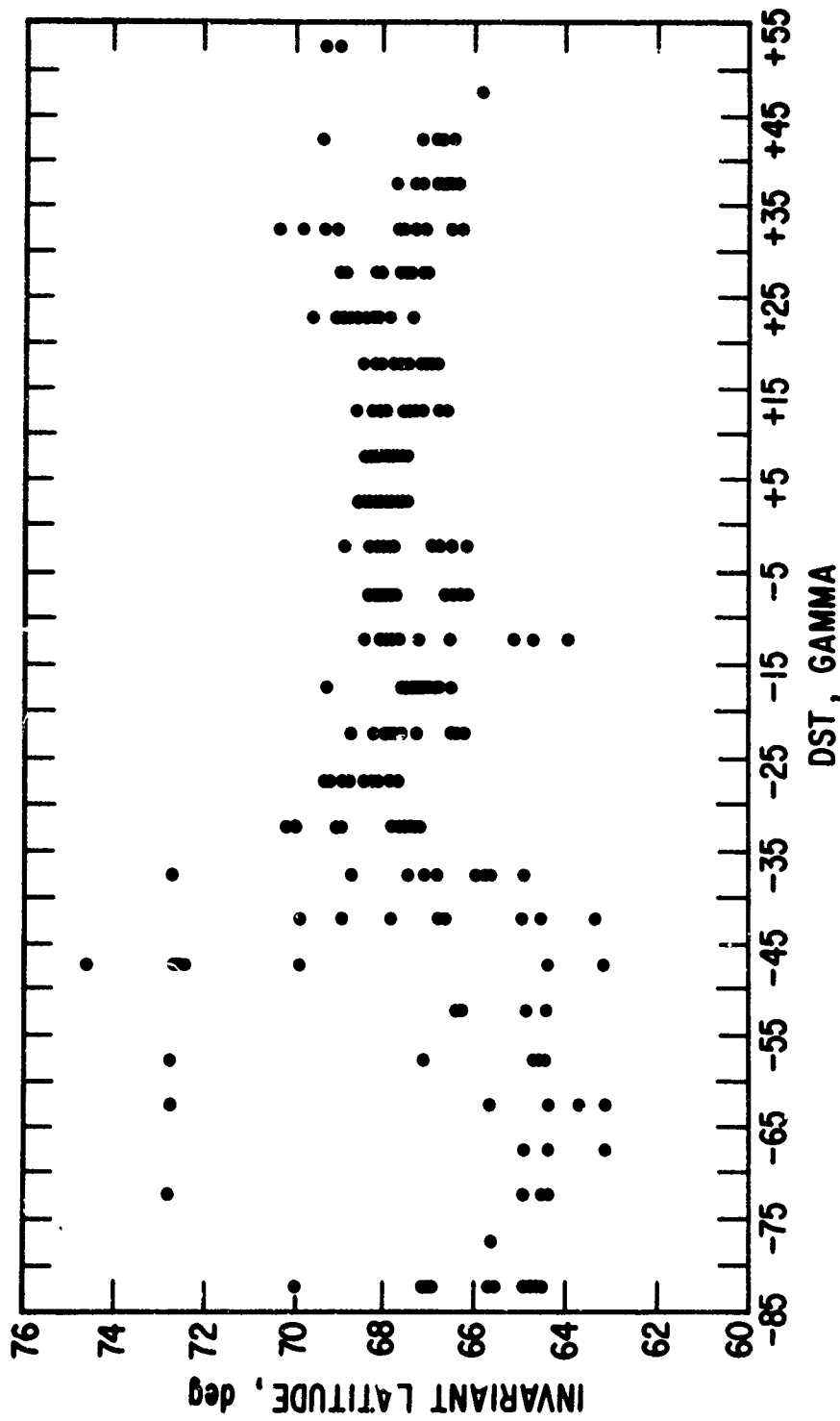


FIG. 27. PLOT OF LOCAL TIME CORRECTED CUTOFFS AVERAGED OVER 5 GAMMA INTERVALS  
versus DST FOR CHANNEL 9 FOR ALL 10 TIME LAGS FROM 5 HOURS BEFORE TO  
5 HOURS AFTER THE OBSERVATION

#### IV. Conclusions

Since the cutoffs appear to be independent of altitude, the data is apparently not seriously biased by background or flux levels. Since the flux levels are functions of altitude or of the distance down the field line at which the point of observation is located, the cutoffs should show a dependence on altitude if the flux levels are influencing them in some systematic way.

The symmetry with respect to the 1100-2300 hr meridian in the plots of  $\Lambda$  versus local time is probably due to the angle of solar wind interaction with the magnetosphere. In 1964, Walters made a quantitative estimate of the angle between the earth-sun line and the axis of solar wind interaction with the magnetosphere. The oblique angle made by the spiral interplanetary magnetic field with radially expanding solar wind was estimated to result in an easterly deflection of the solar wind of from 5 deg to 20 deg. The earth's orbital velocity relative to the radial solar wind direction was estimated to contribute an additional 5 deg. These two effects would cause the axis of symmetry of the magnetosphere to be tilted away from the earth-sun line as if the solar wind comes from a direction 10 deg to 25 deg west of the sun as shown in Figure 28 (Ref. 15:1769). Thus one could expect the local time symmetry axis to be shifted by approximately an hour, as is the case. Strong, however, reports from Vela satellite observations that at  $17 R_e$  only a 2 to 4 deg east-west tilt of the magneto-

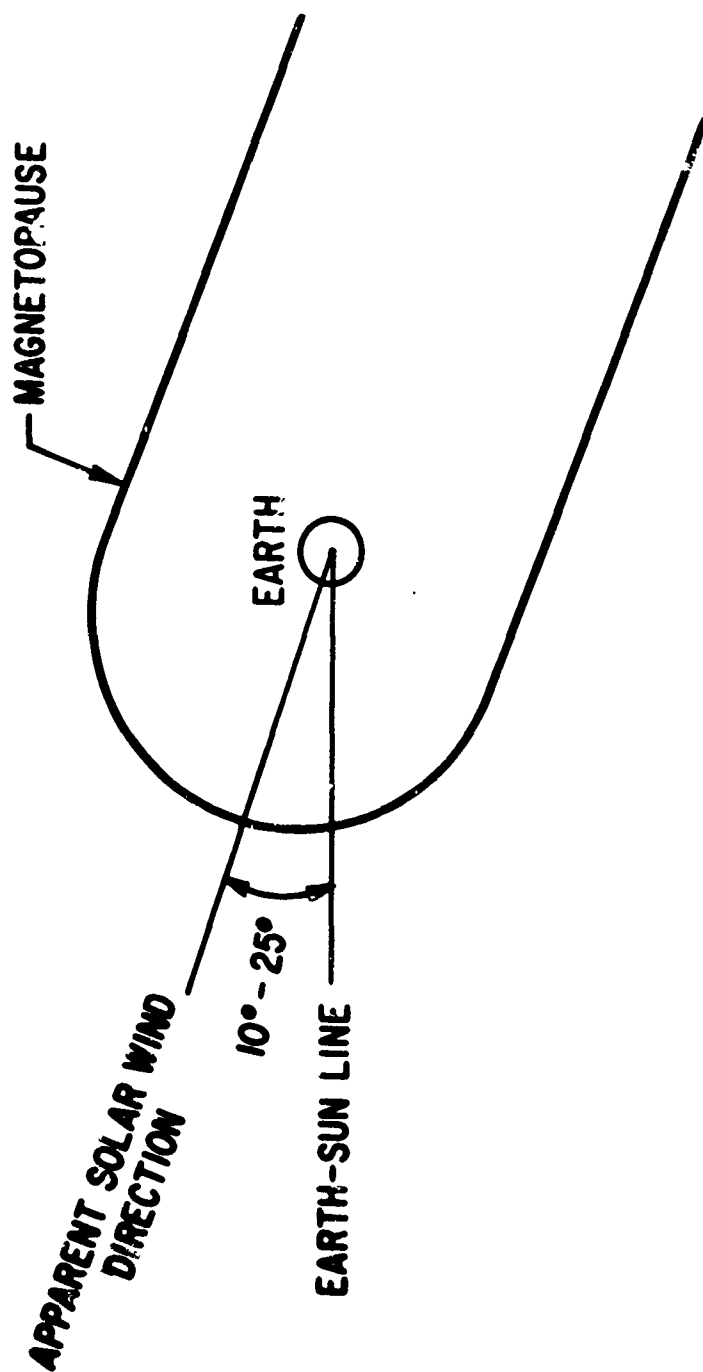


FIG. 28. ANGLE OF SOLAR WIND INTERACTION WITH THE MAGNETOSPHERE

(FROM REF 15:1776)

sphere exists. He predicts this to be the result of the earth's orbital velocity about the sun. The additional tilt from the interplanetary magnetic field does not seem to be present in his data (Ref. 4:377). Thus there is some question as to whether part of the observed shift of the local time symmetry axis is due to the interplanetary field or to some other effect.

No appreciable dawn-dusk asymmetry was detectable in the plots of  $\Lambda$  versus local time. In 1968, when McDiarmid and Burrows reported such a dawn-dusk asymmetry in their data, they were dealing with electrons  $E > 40$  keV, magnetic local time, and periods of little magnetic activity (Ref. 7:49). It is most probable that their asymmetry is caused by electrons with energies between 40 and 225 keV, electrons too low for this instrument. There is also the more remote possibility that the increased scattering of the points from variations in magnetic activity or the use of geographic rather than magnetic local time obscured the effect.

The fact that no relationship between  $K_p$  and  $\Lambda$  was found leads one to conclude that either  $K_p$  is not a good measure of the distortion of the geomagnetic field lines or the 3-hr average value for  $K_p$  is too broad in time to give a good correlation. That  $\Lambda$  seems to show the greatest variation during times of high  $K_p$  indicates that perhaps the latter is true. However, the relationship between  $\Lambda$  and  $K_p$  is still not clear.

The tailing off of the  $\Lambda$  versus Dst plots for large negative values of Dst suggests that Dst may be a good general index for the magnetospheric configuration. However, it does not appear to be accurate as an exact index, since correlations with Dst from several hours before to several hours after the observation yielded essentially the same results. Dst is believed to be mainly due to the establishment of a ring current but also to include the magnetic field due to currents on the interface between the magnetosphere and solar plasma and to some residue of the polar disturbances (Ref. 10:35). Most successful correlations with Dst have been during periods of high magnetic activity. In this study all levels of magnetic activity are considered, and, in fact, the best correlation was obtained for large negative Dst values. If the data were available, one could probably obtain a better and more meaningful correlation by looking at continual cutoff data through a storm as a function of Dst. This, however, would require nearly complete data coverage.

The  $\Lambda$  versus Dst plots appeared about the same for all channels. If Dst can be considered as a general index of magnetospheric configuration, this result suggests that the different energy cutoffs are actually labeling different L shells.

The energies examined in this study are too high to be appreciably affected by electric fields of the magnitude predicted to be present in the magnetosphere. For example, the Taylor and Hones



models predicts fields that would appreciably affect only particles with energies under approximately 100 keV (Ref. 11:3605). Taylor (private communication) suggested that the observed energy dependence of the cutoffs is entirely due to the limiting effect of rigidity on the night side of the magnetosphere. A particle will remain trapped as long as the Lorentz force or stabilizing force from the particle's cyclotron motion is greater than any perturbing force on the particle. However, if the centrifugal force experienced by the particle as it follows the curved lines of the magnetosphere exceeds the Lorentz force, the particle will be scattered in pitch angle and possibly lost. A condition for this loss mechanism to occur is

$$\frac{mv^2 \cos^2 \alpha}{r_c} = \frac{eBv \sin \alpha}{c} \quad (4)$$

where  $m$  is the particle's relativistic mass,  $v$  is its velocity,  $\alpha$  is its pitch angle,  $e$  is its charge,  $B$  is the magnitude of the field,  $c$  is the speed of light, and  $r_c$  is the radius of curvature of the field lines. As eq. (4) indicates, this mechanism becomes important where the radius of curvature of the field lines becomes small, and it affects particles with small equatorial pitch angles, which mirror at high latitudes.

In the magnetospheric models incorporating a current sheet, the field lines on the night side show a kink, which becomes more severe as the first open field line is approached. This effect is shown in Figure 29. The result is that the limiting condition for trapping

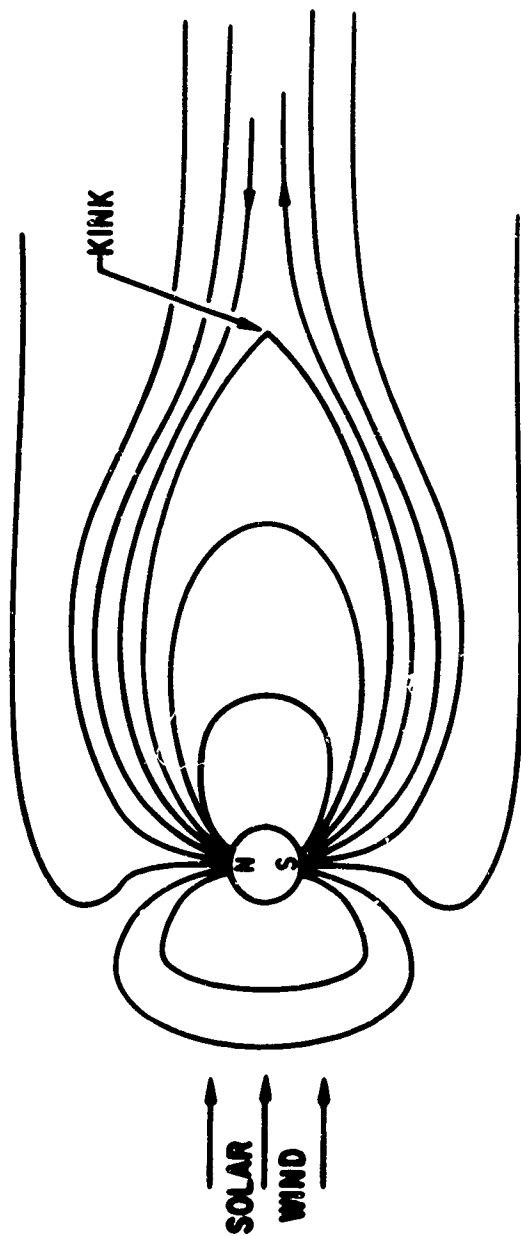


FIG. 29. THE MAGNETOSPHERE SHOWING KINKS IN THE CLOSED FIELD LINES OF THE TAIL  
(FROM REF 12:5137)

occurs at midnight, where the curvature of the field lines is sharpest. In applying the above trapping criterion to his model, Taylor found the theoretical curve shown in Figure 30 for the cutoff as a function of energy. Also shown in Figure 30 is the experimental data from the present study.

The close correlation between the slopes of the observed data and predicted curve supports the conclusion that rigidity is the mechanism causing the observed energy dependence. The difference in magnitude between them probably exists because the model does not accurately define the location of the last closed field line. More recent data from the spectrometer aboard the OV1-14 satellite indicate that the cutoffs for energies below  $\approx 80$  keV begin occurring at constant or lower latitudes. An early malfunction of the OV1-14 has limited the number of orbits of data available, so that no extensive study of it can be made. This early result, however, implies that the  $E > 40$  keV electron cutoffs reported by previous experimenters are associated directly with some energy around 80 keV. The models derived from the  $E > 40$  keV data would be correspondingly affected, in particular the theoretical curve in Figure 30. In any case, the neutral sheet models of the magnetosphere appear valid in that field lines are distorted in the predicted manner.

If the energy dependence is due to rigidity, the lack of an appreciable dawn-dusk asymmetry in the data suggests that there is no

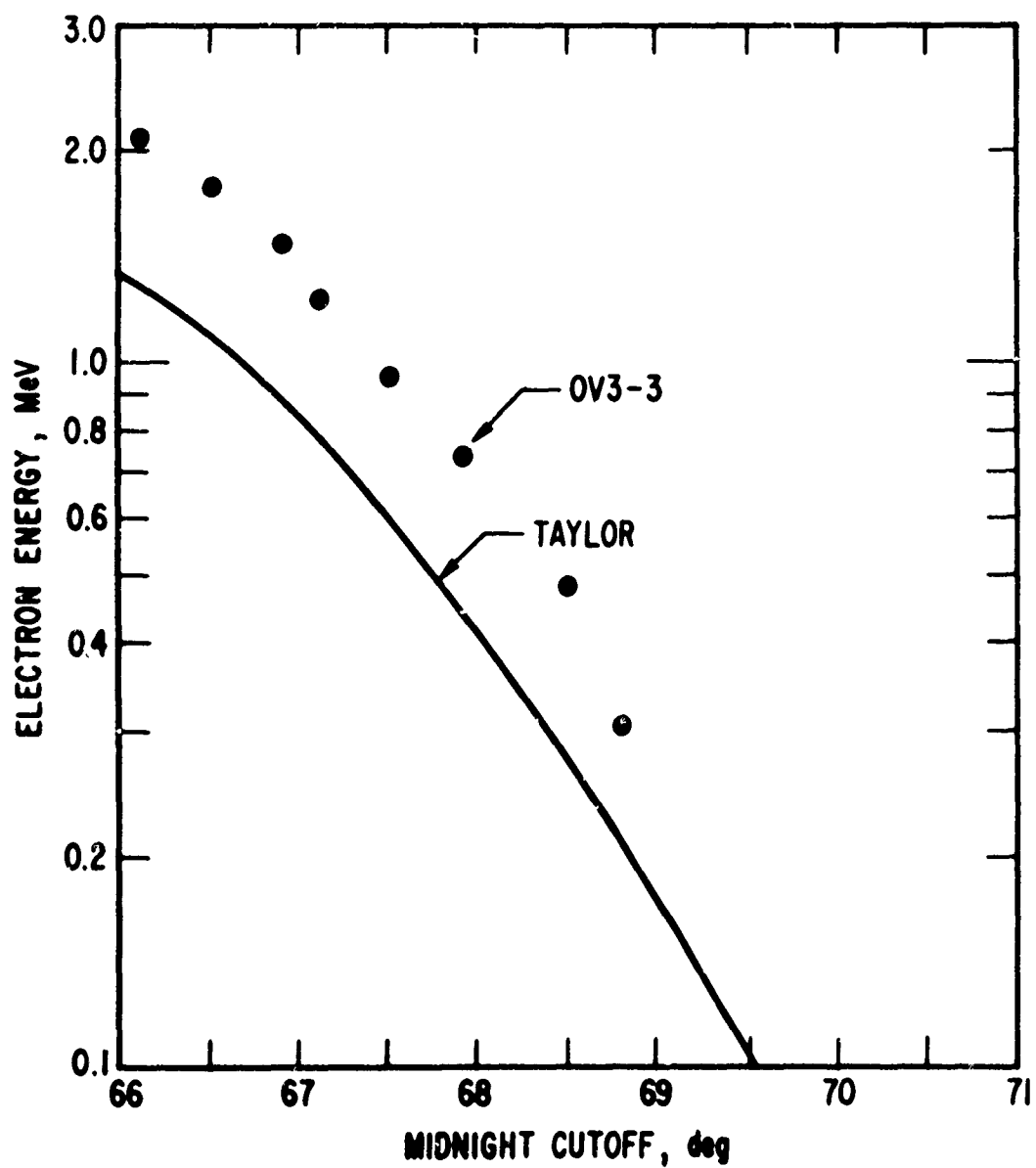


FIG. 30. PREDICTED AND OBSERVED HIGH LATITUDE ELECTRON CUTOFFS AS A FUNCTION OF ENERGY

appreciable source of high energy electrons in the sunlit hemisphere. Also, it appears that energetic electrons do not drift radially an appreciable amount during one drift period.

The apparent dependence of the diurnal variation upon energy is, at least in part, due to geomagnetic field distortion. Figure 31 is a plot of the diurnal variation from the fits to the  $\Lambda$  versus local time plots as a function of the day and night cutoffs for the lowest eight energies. Also plotted are the diurnal variations as a function of the daytime cutoff predicted by Williams and Mead, using a 40  $\gamma$  finite current sheet model, and by the model of Taylor and Hones. If particle drift is independent of energy, the poor correlation between the observed data points and the theoretical curves indicates that these models are not valid in this critical part of the magnetosphere.

Figure 31 shows that, in order to fit the observed data, the true value of the neutral sheet in the models should be somewhere between the two values. However, since the sizes of the neutral sheets are rather large at present as compared to those actually observed, a more correct model could probably be obtained if ring current effects were included. Outside the ring current, field lines would be extended. They would be extended to a greater extent on the nightside hemisphere, producing large diurnal variations without requiring the high intensity neutral sheets presently being used.

(Ref. 16:3027).

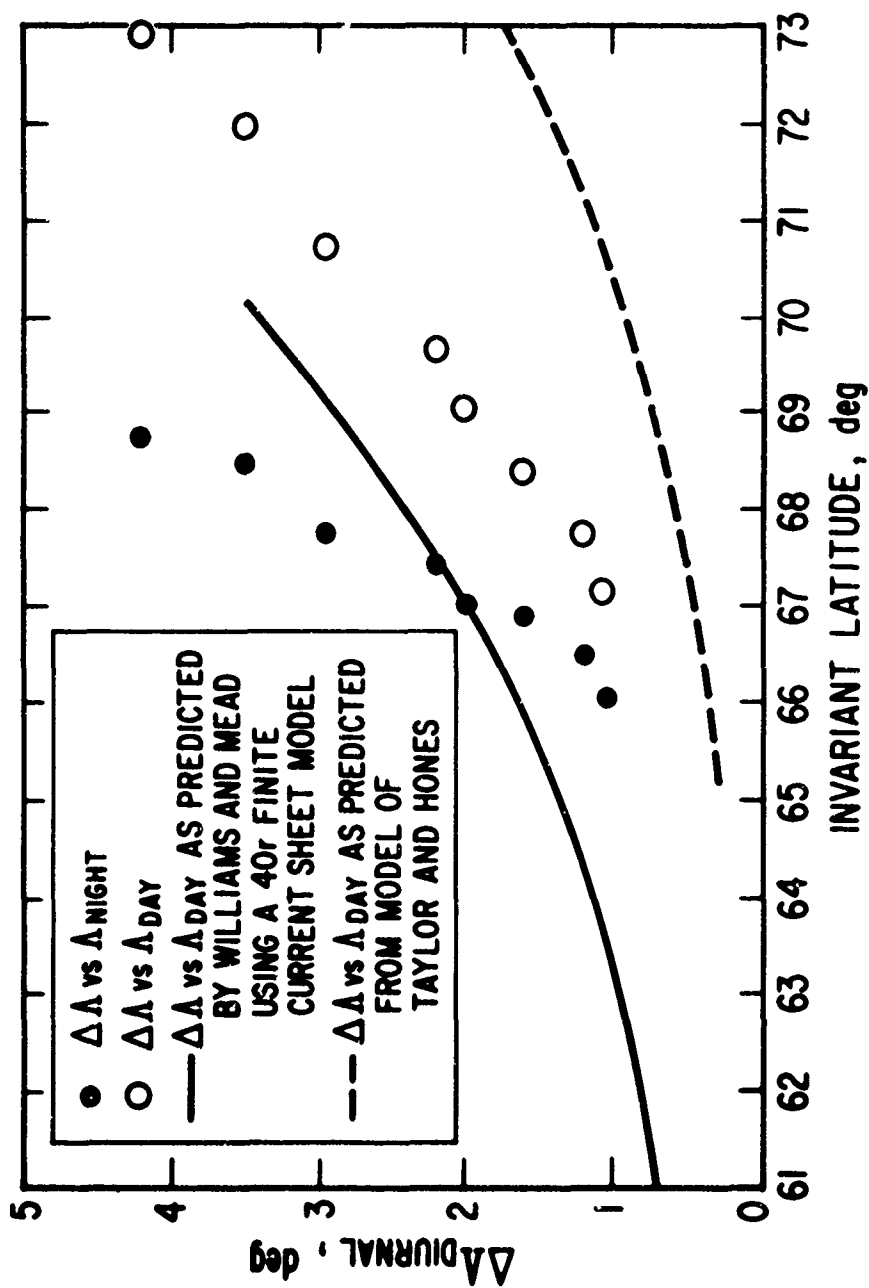


FIG. 31. PREDICTED AND OBSERVED DIURNAL VARIATIONS OF CUTOFFS AS A FUNCTION OF THE DAY OR NIGHT CUTOFF

### V. Suggestions for Future Investigation

Since this study did not reveal any well defined relationship between the high latitude cutoffs and magnetic activity, it appears that some other approaches might be more fruitful. Perhaps with much greater coverage, continual cutoffs could be looked at as a function of energy through a magnetic storm, to determine more exactly what the boundary is doing during disturbed times. Also one could investigate the effect of the ring current more thoroughly by looking at this continual data along with Dst and perhaps even the rate of change of Dst with time.

The mechanism thought by Taylor to be responsible for the observed energy dependence of the cutoff would result in cutoffs that are independent of the maximum outer zone flux. Thus one could test the theory by determining whether a correlation does exist between the cutoff and the maximum flux value. The theory could also be tested by determining the altitude dependence of the cutoff along a field line in the area where the cutoff is observed to occur. Since the loss mechanism is dependent on pitch angle, the flux in the equatorial plane should be well above background on a field line where a high latitude cutoff occurs.

The energy dependence of the diurnal variations in cutoffs left some question as to whether or not particles follow drift paths independent of energy. Construction and examination of isointensity plots

GNE/PH/69-4

should aid in answering this question.

Behavior of the cutoffs as a function of energy for electrons of energy  $E < 225$  keV has not been examined in detail. The OV1-19 should provide the necessary data for such a study. Low energy data is essential for determining electric field configuration in the magnetosphere as well as particle source, loss, diffusion, and acceleration mechanisms.

The high latitude spikes noted in reading off the cutoffs were not investigated in this study. They are real, however, and should be investigated in the future.

The electron flux data used in this study now exists in the form of plots of flux versus L. This introduces the possibility of studying the cutoff mechanism more closely. Such parameters as the slope of the flux versus L curve might be worthy of investigation.



Bibliography

1. Armstrong, T. "Morphology of the Outer Zone Electron Distribution at Low Altitudes from January through July and September 1963 from Injun 3." Journal of Geophysical Research, 70: 2077-2100 (May 1, 1965).
2. Glasstone, Samuel. Sourcebook on the Space Sciences. Princeton, New Jersey: D. Van Nostrand Company, 1965.
3. Green, Alex E. and Philip J. Wyatt. Atomic and Space Physics. Reading, Massachusetts: Addison-Wesley Publishing Company, 1965.
4. Hess, Wilmot N. The Radiation Belt and Magnetosphere. Waltham, Massachusetts: Blaisdell Publishing Company, 1968.
5. Maehlum, B. and B. J. O'Brien. "Study of Energetic Electrons and their Relationship to Auroral Absorption of Radio Waves." Journal of Geophysical Research, 68: 997-1010 (February 15, 1963).
6. McDiarmid, I. B. and J. R. Burrows. "High-Latitude Boundary of the Outer Radiation Zone at 1000 KM." Canadian Journal of Physics, 42: 616-626 (April 1964).
7. McDiarmid, I. B. and J. R. Burrows. "Local Time Asymmetries in the High-Latitude Boundary of the Outer Radiation Zone for Different Electron Energies." Canadian Journal of Physics, 46: 49-57 (January 1968).
8. McDiarmid, I. B. (Private communication: January 10, 1969).
9. O'Brien, B. J. "A Large Diurnal Variation of the Geomagnetically Trapped Radiation." Journal of Geophysical Research, 68: 989-995 (February 15, 1963).
10. Sugiura, Masahisa. "Hourly Values of Equatorial Dst for the I.G.Y." Annals of the International Geophysical Year, Vol. 35, Part 1.
11. Taylor, H. E. and E. W. Hones, Jr. "Adiabatic Motion of Auroral Particles in a Model of the Electric and Magnetic Fields Surrounding the Earth." Journal of Geophysical Research, 70: 3605-3628 (August 1, 1965).

12. Taylor, Harold E. "Adiabatic Motion of Outer-Zone Particles in a Model of the Geoelectric and Geomagnetic Fields." Journal of Geophysical Research, 71: 5135-5147 (November 1, 1966).
13. Taylor, Harold E. (Private communication: February 24, 1969).
14. Vampola, A. L. "Energetic Electrons at Latitudes Above the Outer Zone Cutoff." Journal of Geophysical Research, 74: 1254-1269 (March 1, 1969).
15. Walters, G. K. "Effect of Oblique Interplanetary Magnetic Field on Shape and Behavior of the Magnetosphere." Journal of Geophysical Research, 69: 1769-1783 (May 1, 1964).
16. Williams, Donald J. and Gilbert D. Mead. "Nightside Magnetosphere Configuration as Obtained from Trapped Electrons at 1100 Kilometers." Journal of Geophysical Research, 70: 3017-3029 (July 1, 1965).
17. Williams, D. J., J. F. Arens and L. J. Lanzerotti. "Observations of Trapped Electrons at Low and High Altitudes." Journal of Geophysical Research, 73: 5673-5696 (September 1, 1968).

### Appendix A: The Instrument

The instrument used was the magnetic spectrometer shown in Figure 8. Electrons enter the indicated aperture and are bent by the magnetic field according to their energy. An electron passing perpendicularly through a B field will circle about a field line according to the relation,

$$R_c = \frac{mcv}{eB} = \frac{c}{eB} \left( 2mE + \frac{E^2}{c} \right)^{1/2} \quad (5)$$

where  $R_c$  is the particle's radius curvature,  $m$  is its relativistic mass,  $v$  is its velocity, perpendicular to the field,  $e$  is its electronic charge,  $E$  its kinetic energy,  $c$  is the speed of light and  $B$  is the value of the field. Thus particles of different energies and masses will have different radii of curvature.

The magnetic spectrometer used to acquire the data was of the 180-deg type with nine solid state detectors located at the primary focus. The detectors were 1.0cm x 1.5cm x 1000 $\mu$  thick lithium drifted diodes with a 0.95cm x 1.37cm unshielded sensitive area. Each detector had its own amplifier, two level pulse height analyzer and two log pulserate-to-analog converters with useful ranges from 1 to 10<sup>3</sup> and from 300 to 3.0 x 10<sup>5</sup> pulses per second. All lower thresholds were set at 150 keV and all but one upper threshold were set at 2.65 MeV in order to get uniform bremsstrahlung and penetrating proton background in each channel. The upper threshold in Channel 1 was

set at 2.9 MeV. The energy deposits above 2.65 MeV in Channel 9 were monitored once each second to determine energetic proton contributions. Minimum energy for direct proton penetration is 105 MeV.

Internal baffling around the edges of the uniform field volume on the pole plates acts as a collimator to reduce scattering within the instrument. During calibration no scattered electrons were observed, though bremsstrahlung sensitivity is sufficiently low for the spectrums being investigated and no corrections to the data were necessary.

A 4-MeV Van de Graaff accelerator was used to check energy levels, angular acceptance, and bremsstrahlung sensitivity. Detector efficiencies were determined using electrons from  $\text{Ru}^{106}$  source in a laboratory 180-deg magnetic spectrometer. Protons up to 150 MeV were used to determine the instrument response to penetrating energetic protons. Final calibration of energy levels and geometric factors was done by trajectory analysis on a computer using the measured field and fringing field geometries and the physical dimensions of the instrument. Actual particles were used to verify the computer-generated energy-angle response curves. The various characteristics of the nine channels appear in Table III. All internal voltages, detector currents, and internal temperatures are sampled once each eight seconds primarily to determine the state of the detectors. No changes have yet been observed, probably due to the high thresh-

TABLE III. Characteristics of Detectors

Detector	CENTER E(MeV)	$\Delta E$ (MeV)	Geometric Factor ( $\text{cm}^2 \text{ ster}$ )
1	2.31	0.325	$2.27 \times 10^{-2}$
2	2.04	0.320	$2.48 \times 10^{-2}$
3	1.77	0.310	$2.77 \times 10^{-2}$
4	1.49	0.322	$3.10 \times 10^{-2}$
5	1.225	0.300	$4.17 \times 10^{-2}$
6	0.957	0.285	$4.67 \times 10^{-2}$
7	0.712	0.275	$5.46 \times 10^{-2}$
8	0.475	0.250	$7.30 \times 10^{-2}$
9	{ 0.300 >105 protons	0.150	$4.63 \times 10^{-2}$

(Ref. 14:3-7)

GNE/PH/69-4

hold for proton penetration. The instrument is still operating as it did in the laboratory during calibration except for Channel 2 which became noisy after 18 months in orbit. The data used in the study was taken well before this malfunction occurred.

The spacecraft was spin-stabilized at 8.8 rpm. The particle detector was mounted with its field of view perpendicular to the spin axis and so spin provided a scanning function. An on-board triaxial fluxgate magnetometer provided local magnetic field data which was used to determine pitch angles for the directional data. A 150-minute-capacity tape recorder permitted data to be acquired over an entire orbit (Ref. 14:1254-1256).

## Appendix B: Error Propagation

The errors associated with determining the universal time at which the cutoff occurs are primarily of the random type. The greatest source is the error of judgment associated with finding the cutoffs. Since the amount of error arising from this source is largely dependent upon the sharpness of the cutoff and the density of data points along the curve, it varies according to each reading. To obtain an average standard deviation for all the data would involve the difficult time-consuming task of reading off all the cutoffs several times. Some of the more questionable cutoffs, however, were picked off and the consistency of the readings checked. This showed that the cutoffs as defined had at most an error of  $\approx 30$  seconds due to judgment. The corresponding error in terms of invariant latitude depends on how fast the satellite is moving and where it is at the time the cutoff is determined. On an apogee pass over a pole the 30 seconds would correspond to 0.5 deg invariant latitude while on a perigee pass it could be as high as 2.2 deg.

Another source of random error arises from the ephemeris. The ephemeris for some of the data may be poor and introduces a possible error of up to 10 seconds in universal time and a corresponding error in the cutoff latitudes.

The only known possible source of systematic error is biasing of the data by the observer because of the cutoff shapes. It is

GNE/PH/69-4

possible that the shape of the curve around the cutoff as influenced by the maximum flux and slope influenced the reading in some way. We know of no such error but do introduce the possibility. In any event its contribution is small in comparison to the random sources.



GNE/PH/69-4

Vita

Robert N. Davie Jr. was born on 5 February 1945, in Orange, New Jersey. He received his Bachelor of Science degree from the United States Military Academy in 1967 and was commissioned a Regular Officer in the United States Air Force. His first active duty assignment was the Air Force Institute of Technology.

Permanent Address: 2419 Princess Lane  
Marietta, Georgia

This thesis was typed by Penelope Schwinkendorf.

Unclassified

Security Classification

DOCUMENT CONTROL DATA - R&D		
(Security classification of title, body of abstract and indexing annotation must be entered when the overall report is classified)		
1. ORIGINATING ACTIVITY (Corporate author)		2a. REPORT SECURITY CLASSIFICATION
Air Force Institute of Technology (AFIT-SE) Wright-Patterson AFB, Ohio 45433		Unclassified
		2b. GROUP
3. REPORT TITLE		
ENERGY DEPENDENCE OF HIGH LATITUDE ELECTRON CUTOFFS		
4. DESCRIPTIVE NOTES (Type of report and inclusive dates)		
AFIT Thesis		
5. AUTHOR(S) (Last name, first name, initial)		
Robert N. Davie, Jr. Lt. USAF		
6. REPORT DATE	7a. TOTAL NO. OF PAGES	7b. NO. OF REFS
June 1969	69	17
8a. CONTRACT OR GRANT NO.		8a. ORIGINATOR'S REPORT NUMBER(S)
a. PROJECT NO. N/A		GNE/PH/69-4
c.		8b. OTHER REPORT NO(S) (Any other numbers that may be assigned this report)
d.		
10. AVAILABILITY/LIMITATION NOTICES This document is subject to special export controls and each transmittal to foreign governments or foreign nationals may be made only with the prior approval of the Dean of Engineering, Air Force Institute of Technology (AFIT-SE), Wright-Patterson AFB, Ohio 45433		
11. SUPPLEMENTARY NOTES		12. SPONSORING MILITARY ACTIVITY
13. ABSTRACT		
<p>High latitude electron cutoffs are determined from electron flux data collected by the magnetic spectrometer aboard the polar orbiting OV3-3 satellite (1966-70A). The cutoffs are examined as a function of nine energies from 300 keV to 2.3 MeV and are found to be a function of energy for all local times and to exhibit an energy dependent diurnal variation. This phenomenon is explained with the use of the models of Taylor and Hones and of Williams and Mead.</p>		

DD FORM 1473  
1 JAN 64

Unclassified

Security Classification

14. KEY WORDS	LINK A		LINK B		LINK C	
	ROLE	WT	ROLE	WT	ROLE	WT
outer zone electrons high latitude limit of trapping high latitude electron cutoff energy dependent cutoff						

**INSTRUCTIONS**

1. **ORIGINATING ACTIVITY:** Enter the name and address of the contractor, subcontractor, grantee, Department of Defense activity or other organization (*corporate author*) issuing the report.

2a. **REPORT SECURITY CLASSIFICATION:** Enter the overall security classification of the report. Indicate whether "Restricted Data" is included. Marking is to be in accordance with appropriate security regulations.

2b. **GROUP:** Automatic downgrading is specified in DoD Directive 5200.10 and Armed Forces Industrial Manual. Enter the group number. Also, when applicable, show that optional markings have been used for Group 3 and Group 4 as authorized.

3. **REPORT TITLE:** Enter the complete report title in all capital letters. Titles in all cases should be unclassified. If a meaningful title cannot be selected without classification, show title classification in all capitals in parenthesis immediately following the title.

4. **DESCRIPTIVE NOTES:** If appropriate, enter the type of report, e.g., interim, progress, summary, annual, or final. Give the inclusive dates when a specific reporting period is covered.

5. **AUTHOR(S):** Enter the name(s) of author(s) as shown on or in the report. Enter last name, first name, middle initial. If military, show rank and branch of service. The name of the principal author is an absolute minimum requirement.

6. **REPORT DATE:** Enter the date of the report as day, month, year, or month, year. If more than one date appears on the report, use date of publication.

7a. **TOTAL NUMBER OF PAGES:** The total page count should follow normal pagination procedures, i.e., enter the number of pages containing information.

7b. **NUMBER OF REFERENCES:** Enter the total number of references cited in the report.

8a. **CONTRACT OR GRANT NUMBER:** If appropriate, enter the applicable number of the contract or grant under which the report was written.

8b, 8c, & 8d. **PROJECT NUMBER:** Enter the appropriate military department identification, such as project number, subproject number, system numbers, task number, etc.

9a. **ORIGINATOR'S REPORT NUMBER(S):** Enter the official report number by which the document will be identified and controlled by the originating activity. This number must be unique to this report.

9b. **OTHER REPORT NUMBER(S):** If the report has been assigned any other report numbers (*either by the originator or by the sponsor*), also enter this number(s).

10. **AVAILABILITY/LIMITATION NOTICES:** Enter any limitations on further dissemination of the report, other than those imposed by security classification, using standard statements such as:

- (1) "Qualified requesters may obtain copies of this report from DDC."
- (2) "Foreign announcement and dissemination of this report by DDC is not authorized."
- (3) "U. S. Government agencies may obtain copies of this report directly from DDC. Other qualified DDC users shall request through \_\_\_\_\_."
- (4) "U. S. military agencies may obtain copies of this report directly from DDC. Other qualified users shall request through \_\_\_\_\_."
- (5) "All distribution of this report is controlled. Qualified DDC users shall request through \_\_\_\_\_."

If the report has been furnished to the Office of Technical Services, Department of Commerce, for sale to the public, indicate this fact and enter the price, if known.

11. **SUPPLEMENTARY NOTES:** Use for additional explanatory notes.

12. **SPONSORING MILITARY ACTIVITY:** Enter the name of the departmental project office or laboratory sponsoring (*paying for*) the research and development. Include address.

13. **ABSTRACT:** Enter an abstract giving a brief and factual summary of the document indicative of the report, even though it may also appear elsewhere in the body of the technical report. If additional space is required, a continuation sheet shall be attached.

It is highly desirable that the abstract of classified reports be unclassified. Each paragraph of the abstract shall end with an indication of the military security classification of the information in the paragraph, represented as (TS), (S), (C), or (U).

There is no limitation on the length of the abstract. However, the suggested length is from 150 to 225 words.

14. **KEY WORDS:** Key words are technically meaningful terms or short phrases that characterize a report and may be used as index entries for cataloging the report. Key words must be selected so that no security classification is required. Identifiers, such as equipment model designation, trade name, military project code name, geographic location, may be used as key words but will be followed by an indication of technical context. The assignment of links, rules, and weights is optional.